sustainability

MDPI

Article

GIS-Based Modeling for Vegetated Land Fire Prediction in Qaradagh Area, Kurdistan Region, Iraq

Sarkawt G. Salar [1,*], Arsalan Ahmed Othman [2,3,*], Sabri Rasooli [4], Salahalddin S. Ali [5], Zaid T. Al-Attar [6] and Veraldo Liesenberg [7]

[1] Department of Geography, College of Education, University of Garmian, Sulaymaniyah 46021, Iraq
[2] Iraq Geological Survey, Al-Andalus Square, Baghdad 10068, Iraq
[3] Department of Petroleum, College of Engineering, Komar University of Science and Technology, Sulaimaniyah 46013, Iraq
[4] Department of Forestry, Faculty of Natural Resources, University of Guilan, Someh Sara 41996-13776, Iran; rasooli.sabri@gmail.com
[5] Civil Engineering Department, College of Engineering, Komar University of Science and Technology, Sulaimaniyah 46013, Iraq; salah.saeed@komar.edu.iq
[6] Department of Geology, University of Baghdad, Al-Jadiryah Street, Baghdad 10071, Iraq; bce.19.62@grad.uotechnology.edu.iq
[7] Department of Forest Engineering, Santa Catarina State University (UDESC), Lages 88520-000, SC, Brazil; veraldo@gmail.com
* Correspondence: sarkawt.ghazi@garmian.edu.krd (S.G.S.); arsalan.aljaf@gmail.com (A.A.O.)

Abstract: This study aims to estimate the susceptibility of fire occurrence in the Qaradagh area of the Iraqi Kurdistan Region, by examining 16 predictive factors. We selected these predictive factors, dependent on analyzing and performing a comprehensive review of about 57 papers related to fire susceptibility. These papers investigate areas with similar environmental conditions to the arid environments as our study area. The 16 factors affecting the fire occurrence are Normalized Difference Vegetation Index (NDVI), slope gradient, slope aspect, elevation, Topographic Wetness Index (TWI), Topographic Position Index (TPI), distance to roads, distance to rivers, distance to villages, distance to farmland, geology, wind speed, relative humidity, annual temperature, annual precipitation, and Land Use and Land Cover (LULC). To extract fires that occurred between 2015 and 2020, 121 scenes of satellite images (most of them are scenes of Sentinel-2) were used, with the aid of a field survey. In total, 80% of the data (185,394 pixels) were used for the training dataset in the model, and 20% of the data (46,348 pixels) were used for the validation dataset. Conversely, 20% of these data were used for the training dataset in the model, and 80% of the data were used for the validation dataset to check the model's overfitting. We used the logistic regression model to analyze the multi-data sites obtained from the 16 predictive factors, to predict the forest and vegetated lands that suffer from fire. The receiver operating characteristic (ROC) curve and the area under the curve (AUC) were used to evaluate the accuracy of the proposed models. The AUC value is more than 84.85% in all groups, which shows very high accuracy for both the model and the factors selected for preparing fire zoning maps in the studied area. According to the factor weight results, classes of LULC and wind speed gained the highest weight among all groups. This paper emphasizes that the used approach is useful for monitoring shrubland, grassland, and cropland fires in other similar areas, which are located in the Mediterranean climate zone. Besides, the model can be applied in other regions, taking the local influencing factors into consideration, which contribute to forest fire mitigation and prevention planning. Hence, the mentioned results can be applied to primary warning, fire suppression resource planning, and allocation work. The mentioned results can be used as prior warnings of the outbreak of fires, taking the necessary measures and methods to prevent and extinguish fires.

Keywords: fires; Kurdistan Region; logistic regression; Sentinel-2

check for updates

Citation: Salar, S.G.; Othman, A.A.; Rasooli, S.; Ali, S.S.; Al-Attar, Z.T.; Liesenberg, V. GIS-Based Modeling for Vegetated Land Fire Prediction in Qaradagh Area, Kurdistan Region, Iraq. *Sustainability* **2022**, *14*, 6194. https://doi.org/10.3390/su14106194

Academic Editor: Ivo Machar

Received: 2 April 2022
Accepted: 17 May 2022
Published: 19 May 2022

1. Introduction

Vegetated lands are important geomorphological phenomena. They play a significant role in surface processes, such as erosion and landslides [1–3]. Vegetation is a vital natural resource, which aids in the preservation of environmental balance [4]. Wildfires are the greatest serious hazard to the world's grasslands and forests, causing severe ecological, economic, and social consequences [5]. Wildfires may occur as a result of long dry seasons; however, the majority of these events are caused by anthropogenic actions, such as accumulated fuel load in unmanaged vegetated environments as well as vegetation removal and clearing for increased pasture and agricultural lands [5,6]. They have not, yet, been described adequately because of the complexity of the processes determining fire behavior, the great amount of data required, and the difficulty of the extraction and collection of the data [7]. Every year, wildfires cause a great deal of damage to natural vegetation, property, the biotic elements of a given ecosystem, and the environment itself, thereby threatening people's lives and significant human resources [8]. Fire leads to environmental degradation, by reducing vegetation coverage and, consequently, food resources for fauna, while modifying soil properties leading to degradation, mass movement, and diversity exhaustion [9].

It is vital to identify the factors affecting the spread and occurrence of fires in vegetated areas, to reduce the fire risk in a given environment [10]. Generally, the causes of fires in the vegetation include natural (environmental) and artificial (anthropogenic) factors. Environmental factors affecting fire include biological, physiographic, and climatic factors [11]. Vegetation is one of the most common biological factors affecting fire occurrence, which exerts its effects depending on the species, density, humus, and moisture [12–16]. The factor of topography is composed of the sub-factors of slope, aspect, altitude, plan curvature, and Topographic Position Index (TPI). TPI is another vital factor affecting fire occurrences [17–21].

Among climatic factors, temperature increases, relative humidity decreases, precipitation amounts, and wind speed and direction affect fire occurrences [19,22,23]. Aside from natural factors, anthropogenic factors as fire ignition sources have caused many fires worldwide [24,25], such as roads, farmlands, and residential areas located within or around forests [14,26,27]. In addition, many fires are produced as a means of clearing lands for agriculture or afforestation purposes [28–30]. Therefore, we carried out an inventory of previous research that has a similar topographic environment to the study area, to select the effective factors in fire occurrence. These factors can be divided into two categories: environmental and anthropogenic factors. Environmental factors include slope, slope aspect, elevation, topographic Wetness Index (TWI), TPI, annual temperature, precipitation, wind speed, Normalized Difference Vegetation Index (NDVI), distance from streams, relative humidity, and geology. On the other hand, anthropogenic factors are the distance from roads, the distance from settlements, the distance from farmlands, and LULC.

Various studies have been done on the factors affecting fire intensity and occurrence [2,5,31–36]. The geographical distribution of fires in central Spain has been studied, in terms of environmental factors. This study showed a significant relationship between the area of the burned regions and the topography of those regions. In the same vein, Lozano et al. [37] showed a high correlation between fire occurrence and environmental factors on different geographical scales. Zumbrunnen et al. [38] showed that climate, roads, and livestock play a significant role in fire occurrence in Switzerland. In addition, a non-linear relationship was established between fire occurrence and anthropogenic factors, with the fire occurrence rate being higher in warmer climates. In another study led by Justus [39], the vital factor affecting forest fire distribution is topography, followed by anthropogenic factors.

Humans cannot control fire completely, but they can reduce its intensity and the damage to natural resources, to a great extent. To this end, each area can be zoned, given the points available in terms of fire likelihood. In other words, areas with high fire likelihood must be identified; then, necessary measures should be adopted to prevent or fight fires [40,41]. Several studies have been conducted, so far, to model and assess fire risks in the world, using different methods [42–45]. These studies have used the analytical hierarchical process (AHP) [2,5,11,13,43–45], fuzzy methods [21,46–49], Analytical Network Process (ANP) [50], logistic regression [51–54], artificial neural networks [20,55], support vector machine c, and random forests [15,56] to model fire risks. These methods require accurate preparation and implementation of the produced models, for the factors affecting fire occurrence. Given the complexity of the fire processes in various regions and the effects of various factors on its occurrence, each of the mentioned methods has potential and limitations. Moreover, in many cases and places, researchers may not have the necessary efficiency for the accurate prediction and geographical zoning of fire risks [57]. Therefore, examining the capabilities of these methods and employing them in different regions can help with choosing the best and most effective method. Moreover, the use of the capabilities of the Geographic Information System (GIS) and remote sensing has facilitated the zoning and modeling of fire occurrence [2,12,14,47,58].

In recent years, frequent fires have occurred in the vegetated lands of the Iraqi Kurdistan Region. In fact, fires are among the major causes that destroy these vegetated areas, and few studies have been reported so far. Thus, given the limited natural resources, including shrublands, in this region, the importance of trying to protect them against fires is maximized. However, despite the occurrence of frequent fires, no research has been conducted on the factors affecting the occurrence, intensity, and distribution of fires in this region. Accordingly, in this study, the shrublands of the Qaradagh area were studied, as a sample of the Kurdistan Region forests. Our study investigates the effects of natural and anthropogenic factors on fire risks, by integrating satellite images, logistic regression, and GIS techniques. Therefore, fire risk potentials were mapped and modeled. Preparing the map of fire potentials using a suitable method plays an important role in understanding and predicting fire occurrence in vegetated areas of this region, thereby helping environmental agencies, farmers, and land managers to prevent and deal with this problem through better supervision of their natural resources.

2. Materials and Methods

2.1. Study Area

The Qaradagh area encompasses the southern part of Sulaymaniyah governate, in the Kurdistan Region of Iraq (Figure 1). It is an important area in terms of ecology, biodiversity, and recreation, extending along with the two-mountain series from the northeast to the southeast. The Qaradagh, Sagrma, and Gulan mountain series (anticlines) forms the southern and western parts of the region, while Baranan Mountain (anticline) forms the northern and eastern parts. The region's altitude ranges between 337 m and 1853 m above sea level. This region has a Mediterranean climate [59,60]. According to data from the Tropical Precipitation Measuring Mission (TRMM), for the period of 1998 to 2017 [61], the average annual precipitation of the study area varies between 591 and 703 mm; whereas, the average annual temperature varies between 17 and 19 °C, for the period of 1979 to 2014 [62].

Fires constitute one of the most important challenges that threaten the ecosystem and biodiversity in the Qaradagh area. Through the available satellite images of fires (between May 2015 and October 2020), we surveyed the area and recorded (660) vegetation fires (Appendix B). As a result, 12.35% of the whole study area was exposed to fire during the mentioned period. Sagrma Mountain, at the western part of the study area, was exposed to fire five times, whereas Baranan Mountain, at the eastern part of the study area, was subjected to fire four times.

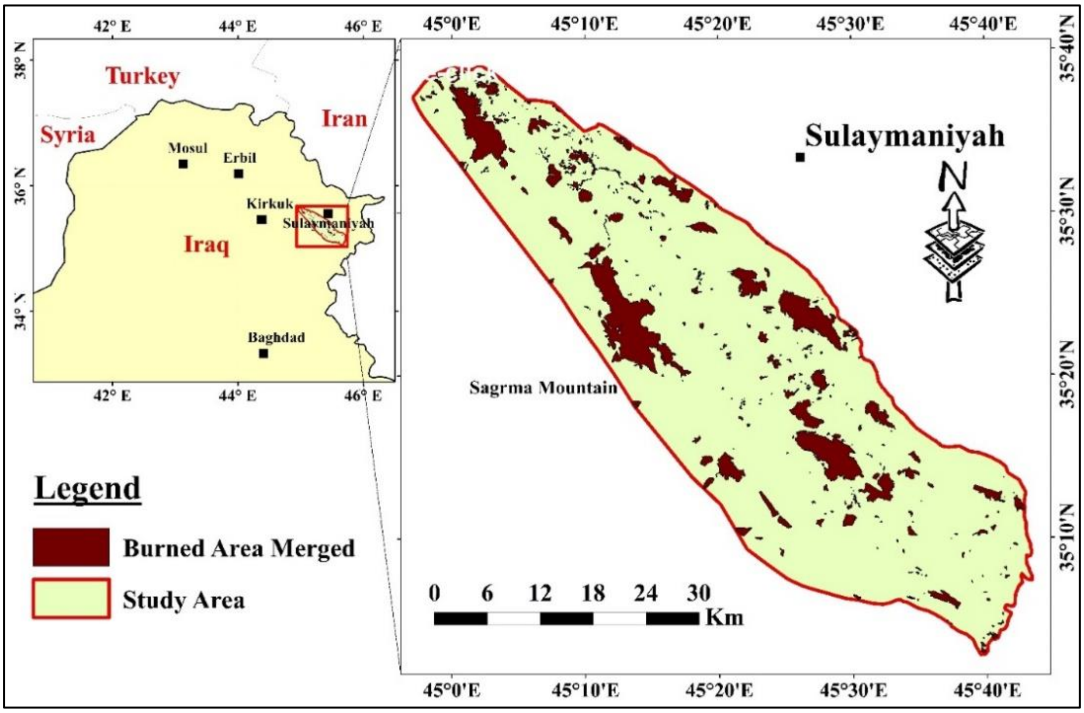

Figure 1. Location of the study area in the southern part of the Sulaymaniyah governate in the Kurdistan Region of Iraq. The total burned area mapped is shown for the entire region.

2.2. Material and Factors Affecting Fire Susceptibility

Many natural and socioeconomic factors affect fire susceptibility in vegetated and pastures of a region, with the impact of each of these factors being specific and different in each region [49]. However, due to the large number and high variety of the factors affecting fire occurrences and data availability, and, also, to facilitate the better modeling and understanding of the calculation process, part of these factors—the main factors affecting fire occurrences in shrublands and pastures—are selected. In the present study, the factors were selected after the comprehensive review of 57 papers (Appendix A) selected from the Scopus (Elsevier) database and related to fire susceptibility in forests and pastures in different countries, published between 2008 and 2020. Accordingly, 16 predictive factors, confirmed in most sources, were employed to produce a fire susceptibility map.

In general, the factors effective in fire occurrence in this study were divided into two categories: environmental and anthropogenic factors. Environmental factors include slope, slope aspect, elevation, Topographic Wetness Index (TWI), TPI, annual temperature, annual precipitation, wind speed, NDVI, distance from streams, relative humidity, and geology. On the other hand, anthropogenic factors are the distance from roads, the distance from settlements, the distance from farmlands, and LULC. From among the aforementioned factors, the three discrete factors, i.e., slope aspect, LULC, and geology, are classified into 9, 5, and 10 classes, respectively. Thus, each class in these three factors is considered a variable, and the total number of layers was 37 factors.

We selected the factors used in the previous papers at the rate of $\geq$10% (16 factors for this study). In other words, we eliminated factors decreasing the accuracy of vegetation fire susceptibility mapping and retained those increasing it.

The required and available information were employed, in light of the factors impacting vegetation fires that were discovered and mentioned (Figure 2). In total, 121 pieces of Sentinel-2 images were downloaded from the EO-Browser website, to map burned areas at their burning time, during the period 2015–2020. The Sentinel-2 imagery was utilized to determine the NDVI, using Sentinel Application Platform (SNAP) software (Table 1). NDVI is defined based on Equation (1) [63]:

$$\mathrm{NDVI} = \frac{\mathrm{NIR} - \mathrm{R}}{\mathrm{NIR} + \mathrm{R}} \tag{1}$$

where NIR and R values are the infrared and red portion of the electromagnetic spectrum, respectively.

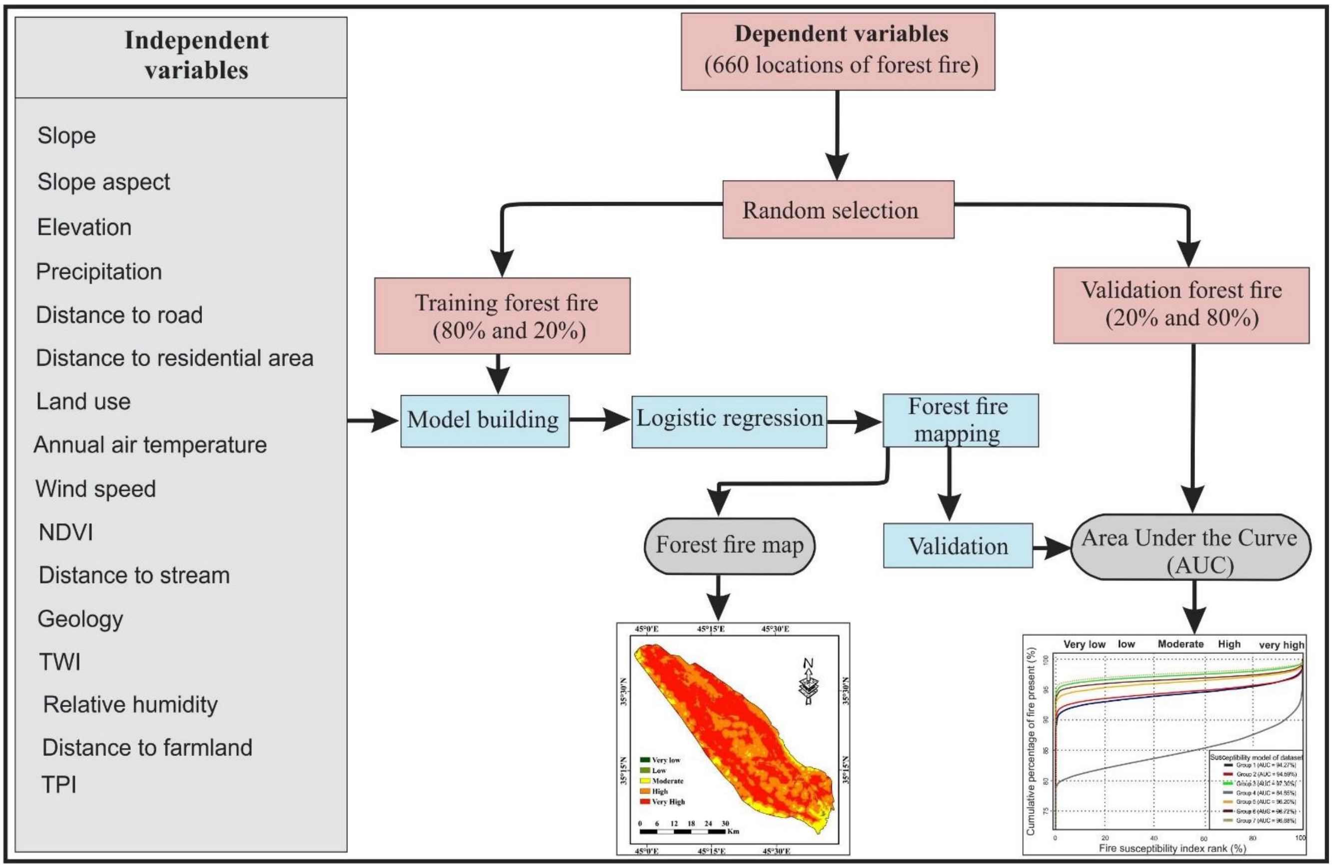

Figure 2. Flow chart of used methodology in vegetation fire mapping.

Table 1. Sentinel-2 spectral bands used to determine the NDVI.

Bands	Central Wavelength (μm)	Resolution (m)
Band 4—Red	0.665	10
Band 8—NIR	0.842	10

In addition, the Digital Elevation Model (DEM) of the Shuttle Radar Topography Mission (STRM), with 1 arc-second resolution, was employed to derive slope, slope aspect, elevation, TWI, and TPI maps. The TWI and TPI are defined, based on Equation (2) [64] and Equation (3) [65], respectively:

$$\mathrm{TWI} = \ln\left(\frac{\alpha}{\tan\beta}\right) \tag{2}$$

$$\mathrm{TPI} = \mathrm{E_c} - \left(\frac{1}{\mathrm{nM}} \sum\nolimits_{\mathrm{i} \in \mathrm{m}} \mathrm{E_i}\right) \tag{3}$$

where α is the area of the drained zone, and tan β is the slope angle in degrees. Where E_c is the elevation of the central pixel, E_i is the elevation of the grid within the local window, and n is the total number of surrounding points employed in the evaluation.

Moreover, GIS world imagery was used to create the road, settlements, and farmlands maps, to extract the maps of distance from roads, distance from settlements, and distance from farmlands. More details of the datasets used and their specifications are fully described and presented in Table 2. Figures 3 and 4 show the 16 predictive factors, which were used in this study.

Table 2. Factors and sub-factors effective in fires as well as their source.

	Factors	The Method of Affecting Fires	Factors Used by Experts (%)	Source
1.	Slope gradient	Fire spread is higher on steep slopes, so that with a 10-degree increase in the slope angle, the propagation speed doubles [66].	54.24	DEM-30 m https://earthexplorer.usgs.gov/ (accessed on 13 August 2021)
2.	Slope aspect	Since southward slopes are warmer and drier than other areas, fire risks are higher on these slopes [67].	52.54	DEM-30 m https://earthexplorer.usgs.gov/ (accessed on 13 August 2021)
3.	Elevation	Under normal conditions, at lower and middle altitudes of an area, fires are much more probable to occur than at higher altitudes because of relatively higher temperatures, lower humidity, and ease of human access [12]. Besides, by an increase in the altitude, damage caused by fires is reduced due to the slower growth of trees compared to lands of lower altitudes and the lower accumulation of resin under the bark [68].	50.85	DEM-30 m https://earthexplorer.usgs.gov/ (accessed on 13 August 2021)
4.	Precipitation	Precipitation is an important factor contributing to the high humidity of fuels, so it is considered a negative indicator of fire spread. In fact, the higher the moisture content in a species' tissue, the more heat and the longer time it will need to evaporate the moisture content, so the higher fire resistance will be. Therefore, the moisture content of the burnable matter is one of the major factors effective in fire occurrence [16]. Besides, rising precipitation in spring increases vegetation growth. This vegetation dries in summer and makes fire occurrence possible [53]. Thus, it is required to pay attention to the amount of precipitation, the precipitation season, and the system creating it. This is because precipitation accompanied by strong lightning can cause fires.	40.68	TRMM-NASA

Table 2. *Cont.*

	Factors	The Method of Affecting Fires	Factors Used by Experts (%)	Source
5.	Distance from roads	When the distance from roads increases, fire risks decrease because of less traffic and human activity [47].	40.68	World Imagery-GIS base map
6.	Distance from settlements	There is a higher fire occurrence risk in the vicinity of settlements involving human activity [58].	40.68	World Imagery-GIS base map
7.	LULC	The effects of LULC are exerted by human activity. Thus, it uses in which there is more human activity with suitable conditions for fire, it is more probable to occur [69].	38.98	LULC https://earthexplorer.usgs.gov/ (accessed on 13 August 2021)
8.	Annual temperature	Temperature rises increase evaporation and transpiration, thereby drying combustible materials, which is considered one of the factors effective in fire occurrence [70].	38.98	Climate Data https://globalweather.tamu.edu/ (accessed on 13 August 2021)
9.	Wind speed	The higher the wind speed is, the higher the fire intensity will be. This is because when the wind moves the air, more oxygen is transferred to the burning environment [22]. In this respect, if the wind blows from the land, it will have a greater effect on fire intensity.	32.2	Climate Data https://globalweather.tamu.edu/ (accessed on 13 August 2021)
10.	NDVI	Since vegetation is the fuel itself, and NDVI shows the condition of vegetation, this factor has a strong effect on fire ignition and the spread of fire [23].	28.81	Sentinel-2 A https://earthexplorer.usgs.gov/ (accessed on 13 August 2021)
11.	Distance from streams	Human activity (particularly, camping along rivers and springs in summer, monitoring cropland, and, sometimes, visiting by tourists to this area, due to the river and the good weather), could affect vegetation fires. Thus, the increase in people's presence along rivers is one of the serious threats [71].	23.73	World Imagery-GIS base map
12.	Geology	The parent rock determines the soil type. Soil is considered one of the major parameters in describing vegetation fires. Besides, it, indirectly, affects the entire environment of a given region [72]. The soil type demonstrates the effects of the texture and composition of soil substances on fire occurrence [15].	16.95	Iraqi Geological Survey (Scale 1: 250,000) GEOSURV-IRAQ
13.	TWI	The TWI shows the size of saturated areas of runoff generation and the effects of topography on the location. Thus, upon an increase in the value of this index, fire risks decrease [15].	16.95	DEM-30 m https://earthexplorer.usgs.gov/ (accessed on 13 August 2021)
14.	Relative humidity	In dry seasons, with an increase in the temperature as well as a decrease in relative humidity and dryness of vegetation, the probability of fire occurrence and spread increases [73].	13.56	Climate Data https://globalweather.tamu.edu/ (accessed on 13 August 2021)
15.	Distance from farmlands	Since many fires are created for clearing agricultural lands off crop residues or developing them, fire risks are greater near agricultural lands [28]. Traditionally, farmers used the above-mentioned method, which is not seen as a harmful method. On the contrary, it is viewed as a method that increases soil fertility. Nevertheless, the fire sometimes gets out of control, unintentionally.	11.86	World Imagery-GIS base map

Table 2. *Cont.*

	Factors	The Method of Affecting Fires	Factors Used by Experts (%)	Source
16.	TPI	It displays the difference in height between a focal cell and all cells in the neighborhood [74]. In addition, TPI shows that flat areas are not as favorable for fire occurrence as ridges and gentle slopes [5]. Besides, the more positive or negative the curvature is, the more likely the vegetation-fire occurrence will be [4].	10.17	DEM-30 mhttps://earthexplorer.usgs.gov/ (accessed on 13 August 2021)

Due to the low number of climatological stations in the study area, we used the TRMM monthly global precipitation data, from 1998 to 2017 [61], and air temperatures acquired from Climate Forecast System Reanalysis (CFSR), from 1979 to July 2014 [62]. The TRMM data within Iraq and the Kurdistan Region have been used and verified by several researchers, such as [75,76], where their accuracy shows a strong direct relationship with the climatological stations' data (coefficient of determination (R^2) > 0.8). Although the CFSR was not verified before, it was compared to the data obtained from Darbandikhan station, located southeast of the study area (Figure 4A). For this purpose, we used the nearest pixel that was located to the climatological stations. In Figure 4C,D, the R^2 indicates a strong direct relationship (>0.8) between the CFSR and the climatological stations' data. The spatial resolution of the CFSR is ~38 km [77]. The TRMM data have a resolution of 0.1 degrees (~9 km). The TRMM and the CFSR data have been converted to vectors and interpolated with a 30 m spatial resolution.

The geological map was obtained from the Iraqi Geological Survey [78]. Whereas, the LULC and geological maps were derived from USGS EarthExplorer website and GEOSURV-Iraq [79].

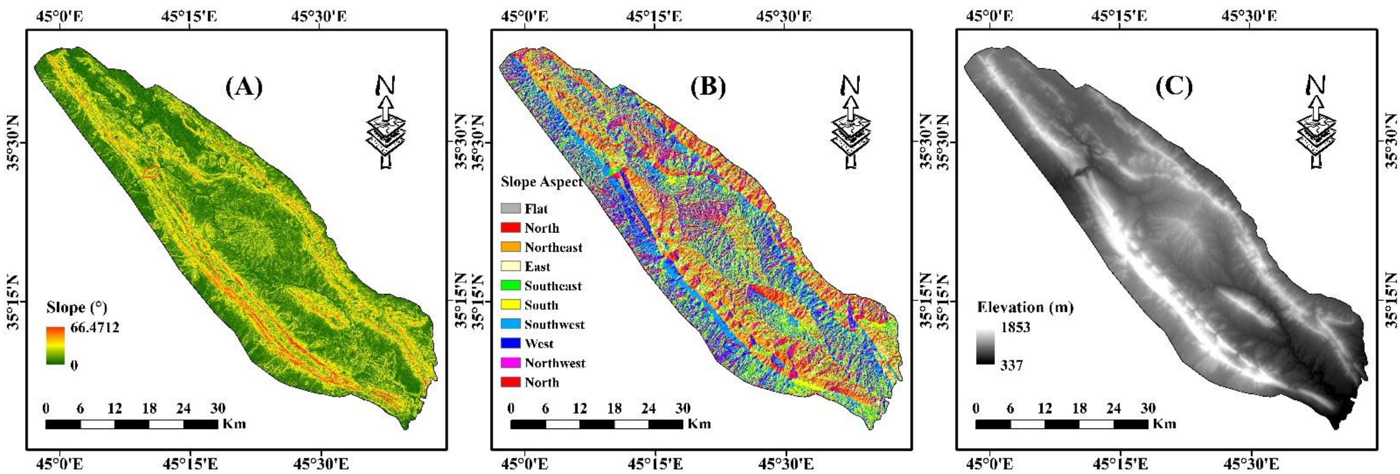

Figure 3. *Cont.*

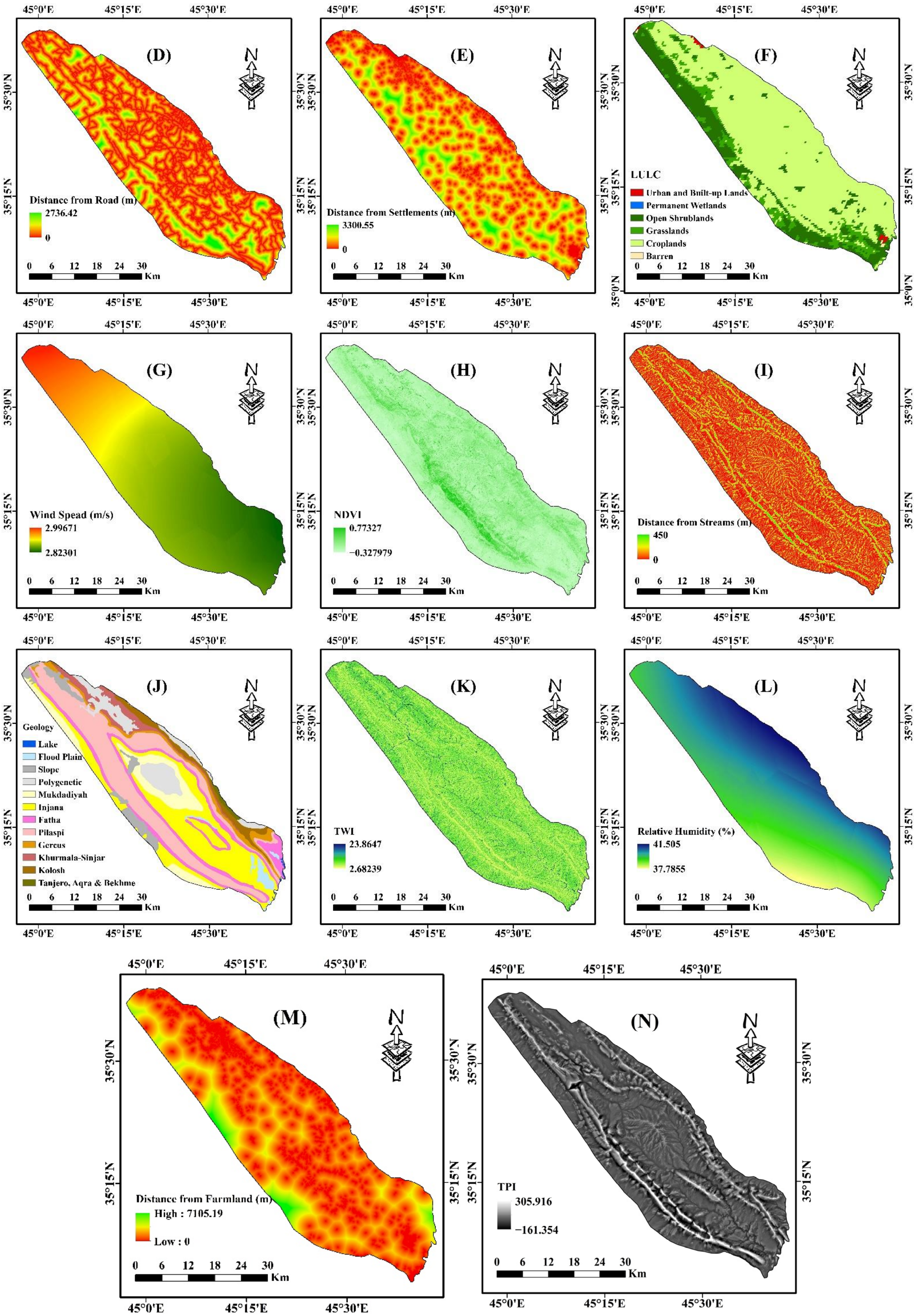

Figure 3. Input vegetation fire factors used in the logistic regression method: (**A**) slope gradient; (**B**) slope aspect; (**C**) elevation; (**D**) distance to the road; (**E**) distance to the settlements; (**F**) land use and land cover; (**G**) wind speed (from 1979 to 2014); (**H**) NDVI; (**I**) distance to the streams; (**J**) geology; (**K**) TWI; (**L**) relative humidity (from 1979 to 2014); (**M**) distance to the farmland; (**N**) TPI.

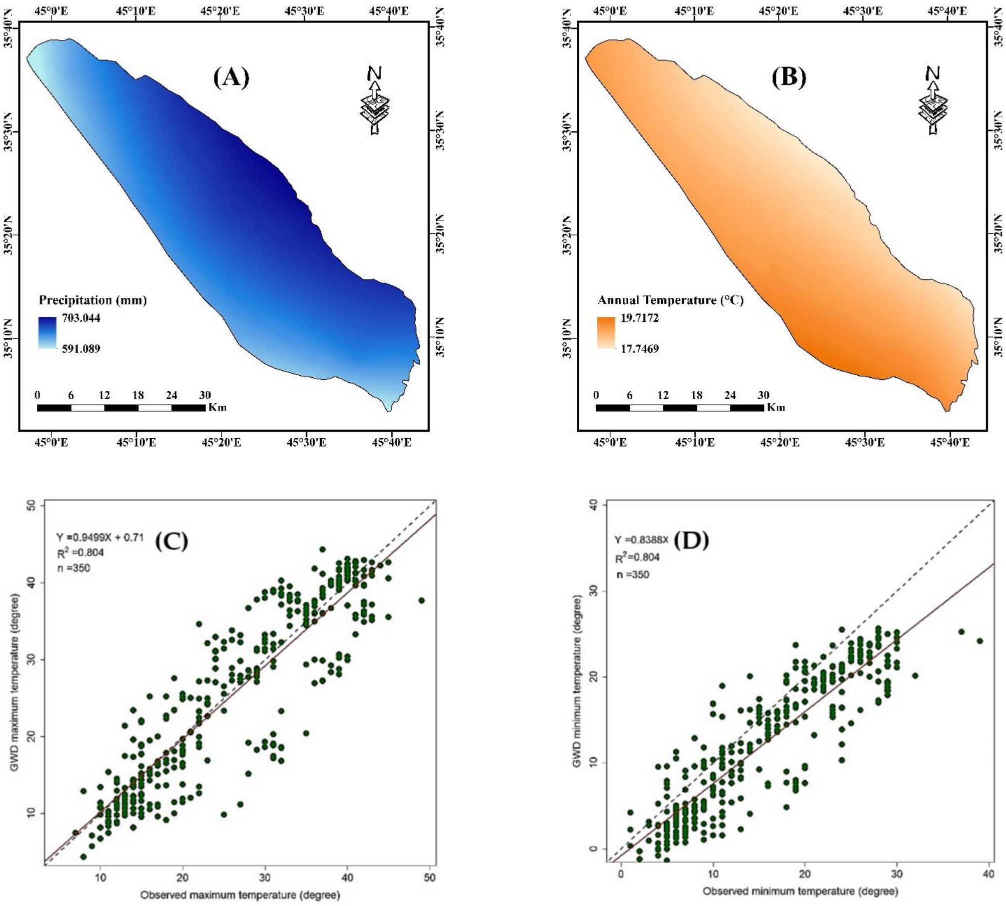

Figure 4. Meteorological parameter maps: (**A**) annual precipitation (from 1998 to 2017); (**B**) annual temperature (from 1979 to 2014); (**C**,**D**) coefficient of determination maximum and minimum temperature, respectively.

2.3. Burn Scar Inventory

A map of past fires is required to investigate the relationship between fire locations and the factors influencing fire occurrence. Thus, the manual delineation of the burn scar inventory was created for 121 satellite images, for the period from 2015 to 2020, in addition to the field studies. These data have been delivered from Sentinel Hub services, which, efficiently, provide long-term analysis. Next, the locations of all burn scars, which occurred during this time interval, were observed on these images, using RGB:432 color composite. Finally, the burn scars were drawn as polygons, and were, thereafter, captured and used for modeling and validation purposes.

When all required data and information were collected from different sources, and after necessary corrections and processing were applied, all factors were converted to the raster format. Moreover, given the fact that the input layers have varied units, which are not suitable as direct inputs for the logistic regression, the input parameters were normalized within the range of 0 to 1 [80]. In the end, making use of the models and coefficients achieved from the logistic regression method, the maps were overlaid with fire risk maps of the study area produced.

2.4. Data Analysis by Logistic Regression

After the parameters were prepared, fire susceptibility maps were prepared, using the logistic regression method. Logistic regression is a statistical method devoted to the group of generalized linear statistical models, which predicts the probability of an event (fires) using independent variables. The key point in logistic regression is that the dependent variable is Boolean (a two-state variable that can be only number 0, meaning non-occurrence, or number 1, indicating the occurrence of an event). Concerning fire probability mapping, logistic regression is used to find the best model for describing the relationships between the presence or absence of a dependent variable (vegetation fires) and a set of independent variables. Logistic regression utilizes the maximum likelihood estimation (MLE) method to find the set of parameters fitting the model best. The model's output yields coefficients between 0 and 1, which through fuzzy theory assigns value 1 to probabilities more than 0.5 (fire occurrence) and value 0 to probabilities less than 0.5 (non-fire occurrence). Finally, it produces a Boolean map for fire susceptibility.

We used the fitting generalized linear models (glm), with a binomial family and logit link in R. Logistic regression is used, by assuming that the probability of the dependent variable being 1 follows the logarithmic curve. Besides, its value is estimated by Function 4 [81], as follows:

$$P\left(y = \frac{1}{X}\right) = \frac{\exp(\mathrm{SBX})}{1 + \exp(\mathrm{SBX})} \tag{4}$$

where, P is the possibility of being 1 for the dependent variables, X represents the independent variables, B is the estimated parameters, and y represents the dependent variables. To linearize the function above, the following transformation is applied:

$$log_e\left(\frac{P}{1+P}\right) = b_0 + b_1x_1 + b_2x_2 + b_3x_3 \ldots + b_kx_k + error\ term \tag{5}$$

where, P is the possibility of being 1 for the dependent variables, $x_1, x_2 \ldots, x_k$ represents the independent variables, b_0 is the coefficient of the regression equation, and $b_1, b_2, \ldots, b_k$ are the coefficients of each independent variable.

This logarithmic change makes the predicted probability become continuous within the range 0 to 1 and makes the model's output be presented as a geographical prediction map for risk probability [82].

2.5. Preparation of Training and Validation Dataset

In total, 103 scenes of satellite images were taken from Sentinel-2, 6 scenes from Landsat-8, and 3 scenes from Landsat-7 (Appendix B). The Landsat images were used to avoid cloudy days and cover the time before the Sentinel-2 launch in 2015. All burned locations, during the mentioned period, were merged to show all areas exposed to the fire on one map. We separated the burned area randomly into training and validation data subsets, as recommended in the literature [83]. A percentage of 80% (185,394 points) was used for the training dataset in the model and 20% (46,348 points) for the validation dataset. A similar number to the training points (185,394 points) from the burned areas were picked at random from the unburned areas. Hence, 185,394 points from the burned areas and 185,394 points from the unburned areas were entered into the model as a training dataset.

2.6. Omission of the Factors Less Effective in Fire Occurrence to Map Fire-Susceptible Areas

To map the fire-susceptible areas, all the training data collected from the 16 main factors were entered as a table into RStudio. The table includes a column that shows the case of the burn scar that exists. An existed burn was coded as 1 and a non-existed burn was coded as 0. The logistic regression model was employed to analyze the data and find the estimation constants (α and β) for probability calculation.

Accordingly, it was observed that in most of the studies, factors, such as slope, slope aspect, and altitude, were used. However, factors such as relative humidity, distance from agricultural lands, and TPI (less than 20% of the reviewed articles) were utilized in fewer studies. Apart from a map, in which all of the mentioned factors were used, we prepared other maps, from which we removed one of the less important factors from the total factors every time. Based on their number of frequencies in the studies, factors of less importance included geology, TWI, relative humidity, distance from farmlands, and TPI. Besides, another map was prepared, from which all six factors were removed. Less important factors were omitted, to stress the importance of the impact of the factors examined on preparing the fire susceptibility map. This is because the careful selection of factors is more important than the methods used for the purpose of zoning [75]. In the end, we will compare the aforementioned maps.

2.7. Validation

Several performance metrics, such as the Roc Curve, Mean Absolute Error (MAE), Relative Error (RE), and Percentage Error (PE) have been used to assess the predictive accuracy of the implemented model in the current study.

Validation or accurate evaluation is required in modeling, to determine the scientific significance or evaluation of a study [3,84]. The efficiency of the model presented in the present study was evaluated, making use of the receiver operating characteristic (ROC) curve and the area under the curve (AUC). This is the most common method used for evaluating modeling efficiency, being used in various research fields [85]. The ROC method is the graphical representation of the balance between the False Positive Rate and the True Positive Rate, for every value of probability. The area beneath the AUC-ROC curve indicates the value predicted by the model, by describing its capability of accurately estimating events or their non-occurrence. In general, an AUC value of 1–0.8 indicates very high efficiency, 0.7–0.8 indicates high efficiency, 0.6–0.7 denotes medium efficiency, and 0.5–0.6 indicates low efficiency, of the model.

In this study, 80% of the fires that have occurred in the study period were used as the training dataset and assigned to model production (Appendix C), while the remaining 20% of the dataset was assigned as a validation. In contrast, we used 20% of the dataset to predict the models (Appendix D), while the remaining 80% of the dataset was utilized to validate the results, to check the model's overfitting.

We used MAE for evaluating the performance of a regression model (Equation (6)). It is a measurable indicator to validate the closeness of predicted values to actual values, as the name suggests [86]. The RE was calculated (Equation (7)), where the ratio of the absolute value to the approximate value is relative error. If the approximate error is unknown, the actual value is used [87]. Equation (8) used the reference value to calculate the PE [88].

$$\mathrm{MAE} = \frac{1}{n}\sum_{i=1}^{n}|P - O| \tag{6}$$

$$\mathrm{RE} = \frac{|P - O|}{O} \tag{7}$$

$$\mathrm{PE} = 100 * \frac{|P - O|}{O} \tag{8}$$

where n represents the represents the number of observations; O represents the actual value; and P represents the predicted value from the susceptibility model.

3. Results

3.1. Vegetation Fire Susceptibility Mapping

After preparing all the factors required and determining the geographical locations of the fires, which took place during the six years within the study area, logistic regression was utilized to determine the relationship between factors affecting fire occurrence and the related spatial modeling. The logistic regression relationship was established between fire occurrences, as dependent variables, and the mentioned parameters, as independent variables. Since the studied factors were selected from the literature review, the regression model was repeated seven times, once to validate the dataset and once, again, to train the dataset to examine the importance of selecting these factors (Appendices C and D). The p-values for all predictor factors used in all models are less than 0.05. Therefore, they have a statistically significant relationship with the fire occurrence in all models. In group 1, we selected those factors that were used in less than 20% of the studies in various regions, which were entered into the regression. In group 2, geology was omitted. Besides, TPI, TWI, and the distance from agricultural lands were removed in groups 3, 4, and 5, respectively. In group 6, relative humidity was omitted, and, finally, all respective factors were entered into the logistic regression in group 7 (Appendices C and D). As a result, seven zoning maps of fire susceptible areas were prepared. The importance of the order of the factors, based on the coefficients achieved in each of the seven cases, is according to the order of the following diagrams, with the maps indicating seven zoning times (Figures 5 and 6).

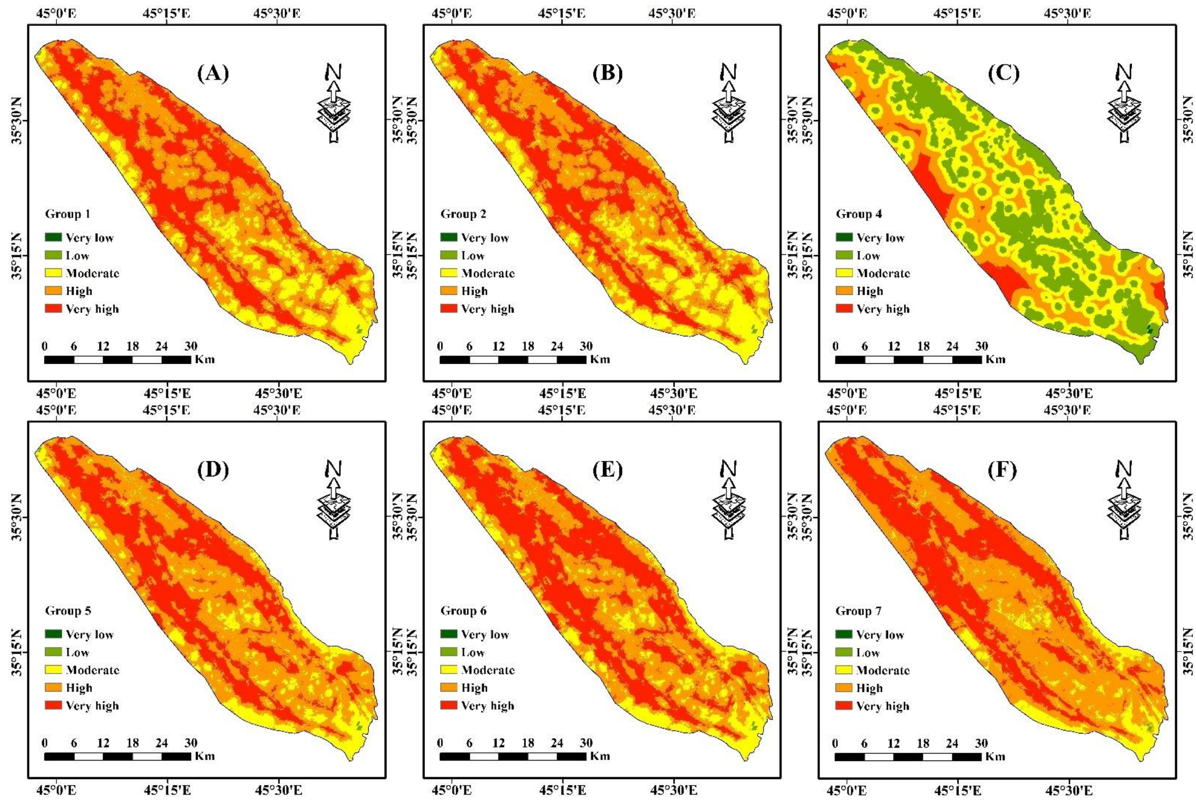

Figure 5. (**A**) fire susceptibility map for group 1; (**B**) fire susceptibility map for group 2; (**C**) fire susceptibility map for group 3; (**D**) fire susceptibility map for group 4; (**E**) fire susceptibility map for group 5; (**F**) fire susceptibility map for group 6.

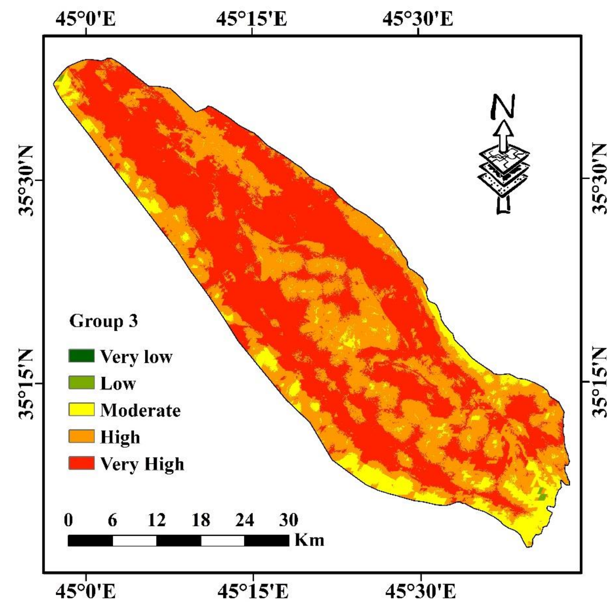

Figure 6. Best fire susceptibility map.

3.2. Validation and Comparison of the Maps

Figure 7 shows the validation results for the fire potential map. This diagram shows that the success rate in all groups is quite apt, ranging from 84.85 to 97.68%. Among all groups, group 3, i.e., the group with TPI excluded from the model calculations, has the highest stability and success rates (AUC), which are 97.30% and 97.31% for both 20% and 80%, as training dataset evaluations, respectively (Figure 7). In addition, when assessing the 20% as a training dataset, group 7 had the highest accuracy (97.68%), compared to the findings of the other groups (Figure 7A), and it came in second place (96.72%) in terms of accuracy, when evaluating the 80% as a validation dataset (Figure 7B), which means less stability than that of group 3.

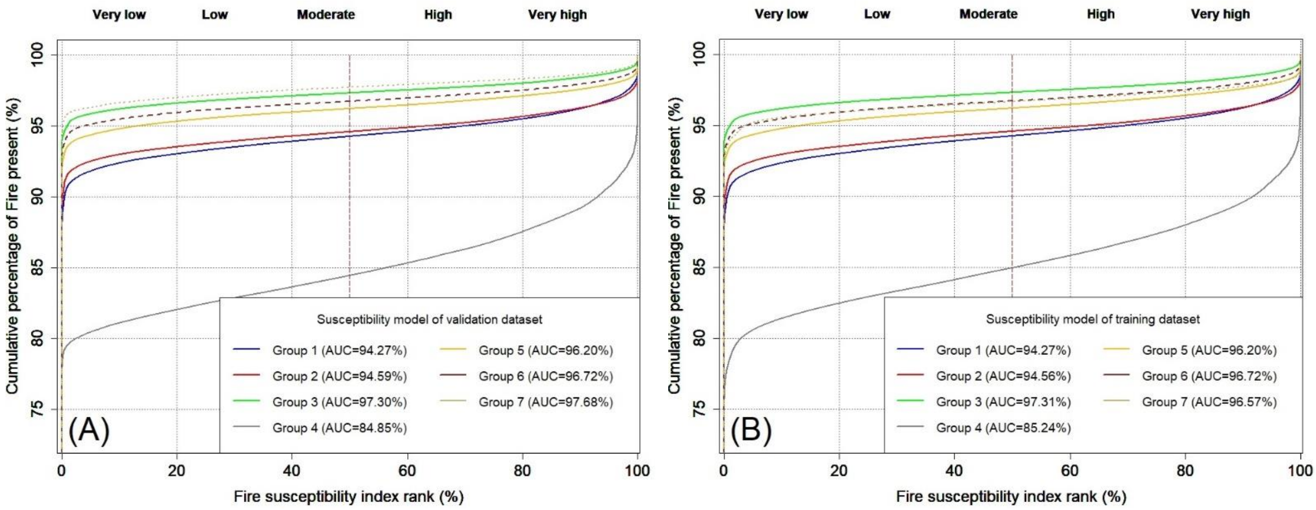

Figure 7. Vegetation fire prediction rate curve, for both (**A**) 20% and (**B**) 80%, as a validation dataset.

The results of the MAE, RE, and the PE of the seven groups show that the best model is group 7. It has a lesser error, while MAE, RE, and PE are 0.62, 2.32, and 0.64, respectively. The worst model (highest errors) come in group 4, where the MAE, RE, and PE are 2.54, 15.15, and 2.99, respectively (Table 3).

Table 3. Additional statistical validation methods.

Validation Method	Group 1	Group 2	Group 3	Group 4	Group 5	Group 6	Group 7
Mean Absolute Error (MAE)%	1.19	1.01	0.68	2.54	0.86	0.76	0.62
Relative Error (RE)%	5.73	5.41	2.69	15.15	3.80	3.28	2.32
Percentage Error (PE)%	1.26	1.07	0.70	2.99	0.89	0.79	0.64

3.3. Key Factor

The predictive ranges of all seven models show that LULC classes, which are related to vegetated areas, are the most common factors that affect fire occurrence (Appendices C and D). This factor includes six classes, which, in order of weight importance, include: cropland, grassland, urban and built-up land, open shrub, and barren area. The wind speed factor has the second-most impact on vegetation-fire occurrence, followed by the geological formations factor, which is composed of clastic sediments (i.e., Tanjero, Aqra, and Bekhme formations).

4. Discussion

4.1. Model Comparison

This study aimed to examine the factors affecting fire occurrence by using the logistic regression method to zone fire occurrence in the Qaradagh area of the Iraqi Kurdistan Region. Based on the AUC of the seven models of the logistic regression (Figure 7), group

3, i.e., the group in which the factor of TPI was not considered, had the highest success stability rate (97.30% and 97.31%) for both evaluations. This reveals that it is not necessary to include the TPI factor in the applied models, to find the susceptible areas to fires. This group ranks second, behind group 7, based on the accuracy results from the MAE, RE, and PE methods, which indicates the effectiveness of all the selected criteria in determining the sensitive areas to fires, as confirmed by the outputs of Figure 7A (97.68%). After groups 3 and 7, the accuracy of all used methods revealed that the values of groups 6 and 5 (excluding relative humidity and distance from agricultural land) were stable, indicating that the effect of the factors on vegetation fires was maintained at the same level and sequence. In terms of stability and sequence, groups 2 and 1 were similar to groups 6 and 5, although with less accuracy, as shown in Figure 7 and Table 3. As for groups 2 and 1 (group 2 with the geology factor removed, and group 1 with all factors that were used in less than 20% of past case studies removed), they were similar to groups 6 and 5 in terms of stability and sequence, but with less accuracy. The low level of accuracy is due to the importance of the geological factor, and its impact on the spatial distribution of plants that are exposed to fires. The accuracy of all the applied statistical methods shows that the least accurate model was represented by group 4, from which the TWI factor was removed. This highlights the effectiveness and strength of the impact of this factor on the accuracy level of the model, which must take into account the extent of its importance. As demonstrated, the values of the statistical accuracy methods show the very strong performance of the models, as well as the selection of apt factors, for preparing a fire zoning map in the studied area. However, it is crucial to be careful enough, when selecting factors affecting fire occurrence. The low success rate in group 4 implies that the factors being more important in fire zoning should not be removed to increase the model's success rate. This methodology is also applicable to other areas with similar geographical and environmental conditions, and decision-makers could benefit from such an approach.

4.2. Factors Impacting Vegetation Fire

The spatial relation strength of affecting and impacting factors on the event was shown by the logistic regression model. It determined the relative importance of each factor influencing the vegetated fire in the study area. Hence, it revealed that the increase in wind speed, NDVI, and geological formation, which includes vegetation, as well as LULC class, which is related to vegetated areas, are the most common factors affecting fire occurrence (Appendices C and D). According to the factor weight results (Figures 5–7), classes of LULC and, then, wind speed gained the highest weight among all groups, with their weight being significantly different from that of other factors. Among LULC classes, the highest weight has been assigned to the cropland class, which can be considered the key factor that enables us to better anticipate and, even, prevent land fires, requiring, therefore, some proper land management practices such as reducing fuel loads periodically and, also, installing firebreaks. Similarly, the results of Pourtaghi et al. [34] show that LULC is the most effective factor in fire occurrence. The presence of adequate fuel is the main cause of most fires occurring in pastures, forests, and agricultural lands. Apart from natural fires in these areas, the role of anthropogenic factors trying to eliminate agricultural residues, repel destructive pests from agricultural products, and speed up the revival of grass species in pastures by creating deliberate fires, is noteworthy. Besides, some unofficial reports relate many wildfires to ethnic disputes, which need more in-depth investigation. Given these reasons, and considering that the highest weight in all seven groups was related to the agricultural land class, one can say that humans are the major cause of fires in this particular region.

After fire occurrence, natural factors can positively or negatively affect fire spread. For example, wind speed is one of the most effective factors in its spread. Besides, wind affects both the fire triangle of fuel, heat, and oxygen as well as the fire behavior triangle of fuel, topography, and climate [89]. Wind, in the fire triangle, transfers more oxygen to the fuel, thereby causing the initial fire spark. On the other hand, the climate factor is seen in the fire behavior triangle, with wind being one of the main components of climate. Wind spreads fire further to surrounding areas and makes its extinguishment more difficult.

The data about wind direction in the study area are poor, as they are missing detailed information. Local winds dominate topographic fires more than prevailing winds, due to slope and differences in the solar heating of the Earth's surface. Forest fires are more sensitive to small changes, so slight differences in topographic winds, slopes, or sides have a greater impact on fire behavior [90]. From the general information, the effect of wind direction on vegetation fires in each pixel is close to equal, in areas characterized by an almost equal geographical distribution of vegetation density; therefore, we ignored the wind direction factor. In the future, we will consider the wind direction factor once local measurements become available for better spatial analysis.

High temperatures, as well as low precipitation and relative humidity, dry the environment, thereby providing suitable environmental conditions for fire occurrence and spread. In regions with these attributes, in case there are combustible materials with, usually, a small amount of humidity, fire occurrence potentials are very high [91]. Due to the fact that two climatic factors, temperature and precipitation, are highly effective in causing fires in terms of time, and given the investigation that was made in the studied area, they cannot cause significant climatic changes in a habitat on such a limited scale. Research on the correlation between fires and soil types indicates that the soil moisture content and its effects on the diversity of plant species are the most effective factors in controlling fire occurrence or non-occurrence [34].

The factors of the distance from roads, residential areas, and rivers reflect humans' role in fire occurrence [92]. These factors can play a dual role in fire occurrence and spread. In the vicinity of these factors, due to more human traffic and activity, fire occurrence is more likely. However, the presence of these factors can be effective in preventing fire spread, after its occurrence. Roads can act as firebreaks, by preventing the fire from spreading to surrounding areas. As fire can be contained by humans, in case it occurs in the vicinity of residential areas, it will be extinguished sooner due to easy human access. In the present study, locations of residential areas were considered as a polygon, not a point, and, then, a map of the distance from these areas was prepared. In other words, one could say that population density has been somehow considered. Accordingly, the higher the population density is, the higher the fire probability will be. In the vicinity of rivers and waterways, due to the higher humidity of combustibles, the fire spread rate decreases [45].

The TPI implies that flat areas are not as susceptible to fire as sloping areas. Moreover, fire occurrence is higher in convex slopes than in concave slopes. This case can be justified, both at the beginning of the fire and at the time of its spread. Humidity is lower in sloping areas, so the fire spread speed increases with increasing the slope angle after fire occurrence. The TWI determines the effects of topography on the rate of saturated surfaces for producing runoff, which plays a significant role in the soil moisture content and slope stability. Hence, there is an inverse correlation between an increase in this index and fire occurrence and spread [93].

The high density of the Gramineae species results in increased vegetation density and the supply of fuels effective in surface fires. Moreover, fire statistics indicate that the highest frequency of fires occurs almost from early summer to early autumn. Given the increasing temperatures, decreased relative humidity, dryness of vegetation in summer, and concomitant effects of human activities, fire is intensified in the region, being consistent with the studies of Gholami et al. [94] and Rafiee et al. [95].

In the Qaradagh area, further work is necessary to estimate the local biomass and total carbon levels, which, in turn, can give an idea of the health of the available crops that could feed random fires. Therefore, we suggested using the method applied by Oliveira et al. [96] to integrate the field-observed biomass data with lidar data from various sensors, to estimate the biomass and carbon levels obtained in the dry vegetated land within our study area. Moreover, lidar metrics can be used to predict wildfires behaviors and risk assessment measures, by combining lidar data with Landsat-derived indices [96,97] to map canopy cover, canopy height, canopy base height, and canopy bulk density as well as to evaluate the aboveground carbon density through shrubland allometric relationships.

Furthermore, the addition of hyperspectral data can be beneficial in terms of distinguishing the moisture content of crops more accurately [98], which, in turn, can act as a predictor of fires rate. The implementation of such data, in addition to our model, will provide holistic yet easy-to-apply methods for agriculture managers, which will aid them in their production rates while minimizing losses through raising awareness on how to combat wildfires.

4.3. Advantages and Disadvantages

One of the major merits of this study is providing information about the statistical weight of every individual variable on the overall result. Moreover, the high accuracy achieved in the present research could have been due to the use of the majority of the factors affecting fire occurrence, which, in turn, allowed the preparation of a more accurate fire susceptibility map. The model's limitation is that the factors impacting the vegetation fire differ in space and time; in other words, the model cannot be applied everywhere, at any time, using the same factors influencing the event. Therefore, this model can be applied in arid and semi-arid mountainous regions. For other regions that have different environments and topography, the priority should be on careful choice of the predictive factors, which is far more significant than the methods utilized. Interestingly, multitemporal measurements of Synthetic Apertura Radar (SAR) and Light Detection and Ranging (LIDAR) are suggested for further studies, to estimate carbon release and better assess soil erosion and vegetation recovery.

5. Conclusions

Fire events, caused by natural or anthropogenic factors, are a major threat to landscape resources, so they must be controlled and prevented. To minimize this threat to forests, managers should be fully knowledgeable about past fire processes. Accordingly, spatial analysis of fires must be performed in every region, and conservation strategies should be formulated for every region, after a thorough understanding of temporal–spatial processes. The prerequisite for such endeavor is the ability to make predictions, perform spatial analyses, and prepare a fire susceptibility map. The use of the logistic regression method is one of the risk-modeling methods, which helps to determine the relationship between independent and dependent variables. Additionally, combining remote sensing data with geographic information data and statistical models permits fire managers and personnel to predict 'where and when' vegetation fires will occur.

In the current study, a fire susceptibility map was prepared for the Qaradagh district, using the logistic regression method. To examine the importance of the factors selected, the regression model was repeated seven times. Each time, one of the factors used less frequently in previous studies was omitted. Moreover, all of the factors were entered once into the regression for modeling. The AUC value was shown to be higher than 96%, in all groups. This indicates the remarkable performance of the model and the selection of suitable factors, for preparing a fire zoning map in the study area. According to the results, to increase the model's success rate, factors less effective in fire zoning should be removed. Based on the coefficients obtained, it was found out that the land-use factor exerted the greatest impact on fire occurrence, among all seven cases, in the current study area.

This approach can be applied to other areas having the same geographical conditions. However, this requires selecting the variables and their weights that work for the tested region, based on its environmental conditions.

More detailed land cover classification (particularly classifying other vegetation types and trees) can increase the understanding and accuracy of vegetated land fire prediction and is encouraged for future studies. Finally, we suggest considering the Qaradagh district as a natural protection area, since forest resources are rare and vegetation fires are high in the Kurdistan region.

Author Contributions: Conceptualization, S.G.S., A.A.O. and S.R.; methodology, S.G.S., A.A.O. and S.R.; software, S.G.S., A.A.O. and S.R.; validation, S.G.S., A.A.O., Z.T.A.-A. and S.R.; formal analysis, S.G.S., A.A.O. and S.R.; investigation, S.G.S., A.A.O. and S.R.; resources, S.G.S. and S.R.; data curation, S.G.S., A.A.O. and S.R.; writing—original draft preparation, S.G.S., A.A.O., S.R. and Z.T.A.-A.; writing—review and editing, S.G.S., A.A.O., S.R., S.S.A. and V.L.; visualization, S.G.S., A.A.O., S.R., S.S.A. and V.L. All authors have read and agreed to the published version of the manuscript.

Funding: This research received no external funding.

Institutional Review Board Statement: Not applicable.

Informed Consent Statement: Not applicable.

Data Availability Statement: Not applicable.

Acknowledgments: We would like to thank the USGS and ESA for their free data, which were used in this study. Moreover, we would like to thank ESA and SEOM (Scientific Exploitation of Operational Missions) for providing SNAP software. V.L. thanks the Brazilian Council for Scientific and Technological Development (CNPq) and the Research and Innovation Support Foundation of Santa Catarina State (FAPESC), for individual support. We are thankful to Ahmed K. Obaid for helping in the discussion.

Conflicts of Interest: The authors declare no conflict of interest.

Appendix A Dependable Factors

References	Slope	Slope Aspect	Elevation or Altitude	Distance from the Residential or Urban Area	Precipitation	Distance from Road	Land Use and Land Cover	Vegetation Cover	Annual Air Temperature	Wind Speed	NDVI	Burned Pixels	Distance from Streams	Soil Type	Plan Curvature	Topographic Wetness Index (TWI)	Relative Humidity	Distance from Agriculture Land	TPI
[2]	*	*	*	*	*	*		*										*	
[4]	*	*	*	*	*	*	*		*	*	*		*	*	*	*			*
[5]	*	*	*	*	*	*				*	*								*
[9]							*												
[12]	*	*	*	*		*													
[13]	*	*		*		*		*											
[14]				*		*	*		*		*		*					*	
[15]	*	*	*	*	*	*	*		*	*	*		*	*	*	*			
[19]	*	*	*	*	*	*	*		*	*	*		*	*	*	*	*		*
[21]	*	*	*	*	*	*	*	*	*	*	*		*	*	*	*			
[22]	*	*	*		*	*	*		*	*	*		*	*	*	*			
[23]	*	*	*	*	*		*		*	*	*						*		
[26]	*	*	*	*	*	*	*		*				*			*			
[34]	*	*	*	*	*	*	*		*	*	*		*	*	*	*			*
[35]	*	*	*		*				*	*					*	*			
[42]	*	*	*					*						*					

References	Slope	Slope Aspect	Elevation or Altitude	Distance from the Residential or Urban Area	Precipitation	Distance from Road	Land Use and Land Cover	Vegetation Cover	Annual Air Temperature	Wind Speed	NDVI	Burned Pixels	Distance from Streams	Soil Type	Plan Curvature	Topographic Wetness Index (TWI)	Relative Humidity	Distance from Agriculture Land	TPI
[43]												*							
[45]	*	*	*	*		*		*										*	
[48]	*	*	*	*	*	*	*		*	*	*								
[50]	*	*	*	*	*	*	*		*	*	*								
[53]	*		*		*				*				*					*	
[54]	*	*		*	*	*	*			*	*					*			
[56]	*	*	*					*							*				*
[58]	*	*		*		*		*										*	
[99]	*	*	*																
[100]								*											
[101]												*							
[102]												*							
[103]												*							
[104]												*							
[105]	*	*	*	*	*	*	*		*			*		*			*		
[106]												*							
[107]								*											
[108]	*	*	*				*	*	*										
[109]							*	*				*							
[110]								*				*							
[111]							*					*							
[112]								*											
[113]												*							
[114]								*				*							
[115]	*	*	*		*	*	*	*	*	*			*		*		*		*
[116]	*	*	*	*		*	*	*											
[117]								*											
[118]	*	*	*	*	*	*	*						*	*	*	*			
[119]								*				*							
[120]								*											
[121]				*				*				*							
[122]												*							
[123]	*	*	*	*	*	*		*	*				*					*	
[124]					*				*	*							*		
[125]			*		*			*	*	*							*		
[126]	*	*	*				*		*	*	*								
[127]	*	*	*	*	*	*		*	*	*			*	*			*	*	
[128]							*				*								
[129]											*								
[130]												*							
[131]	*	*	*	*	*		*		*	*	*						*		
Sum	31	30	29	24	23	23	23	23	22	18	16	16	13	10	10	10	8	7	6
Average rate	54.24	52.54	50.85	40.68	40.68	40.68	38.98	38.98	38.98	32.20	28.81	27.12	23.73	16.95	16.95	16.95	13.56	11.86	10.17

* The factor existed in the paper.

Appendix B Recorded Vegetation Fires during the Period (May 2015 to October 2020)

No.	Year	Month	Day	Date	Imagery	Area (m^2)	No.	Year	Month	Day	Date	Imagery	Area (m^2)
1	2015	5	21	21052015	Landsat-7	27,270	331	2017	9	26	26092017	Sentinel-2	762,500
2	2015	5	21	21052015	Landsat-7	2816	332	2017	9	26	26092017	Sentinel-2	50,670
3	2015	5	21	21052015	Landsat-7	52,620	333	2017	9	26	26092017	Sentinel-2	32,170
4	2015	5	21	21052015	Landsat-7	22,320	334	2017	10	11	11102017	Sentinel-2	24,900
5	2015	5	21	21052015	Landsat-7	63,680	335	2017	11	11	11102017	Sentinel-2	387,900
6	2015	5	21	21052015	Landsat-7	17,650	336	2017	11	11	11102017	Sentinel-2	1,534,000
7	2015	5	21	21052015	Landsat-7	18,490	337	2017	11	11	11102017	Sentinel-2	3992
8	2015	5	21	21052015	Landsat-7	7165	338	2017	11	11	11102017	Sentinel-2	4350
9	2015	5	21	21052015	Landsat-7	7007	339	2017	11	11	11102017	Sentinel-2	989.6
10	2015	5	21	21052015	Landsat-7	13,970	340	2018	6	13	13062018	Sentinel-2	118,000
11	2015	5	21	21052015	Landsat-7	32,250	341	2018	6	13	13062018	Sentinel-2	1,723,000
12	2015	5	21	21052015	Landsat-7	10,980	342	2018	6	13	13062018	Sentinel-2	5774
13	2015	5	21	21052015	Landsat-7	5936	343	2018	6	13	13062018	Sentinel-2	9821
14	2015	6	6	6062015	Landsat-7	42,470	344	2018	6	16	16062018	Sentinel-2	2742
15	2015	6	6	6062015	Landsat-7	3,587,000	345	2018	6	16	16062018	Sentinel-2	4328
16	2015	6	14	14062015	Landsat-8	5524	346	2018	6	18	18062018	Sentinel-2	17,240
17	2015	6	14	14062015	Landsat-8	383,400	347	2018	6	18	18062018	Sentinel-2	11,090
18	2015	6	14	14062015	Landsat-8	94,130	348	2018	6	18	18062018	Sentinel-2	13,350
19	2015	6	14	14062015	Landsat-8	128,600	349	2018	6	18	18062018	Sentinel-2	13,620
20	2015	6	14	14062015	Landsat-8	5757	350	2018	6	18	18062018	Sentinel-2	25,740
21	2015	6	14	14062015	Landsat-8	129,000	351	2018	6	21	21062018	Sentinel-2	11,070
22	2015	6	14	14062015	Landsat-8	7679	352	2018	6	23	23062018	Sentinel-2	85,820
23	2015	6	14	14062015	Landsat-8	1,021,000	353	2018	6	23	23062018	Sentinel-2	20,690
24	2015	6	14	14062015	Landsat-8	758,00	354	2018	6	23	23062018	Sentinel-2	42,380
25	2015	6	14	14062015	Landsat-8	148,600	355	2018	6	23	23062018	Sentinel-2	17,320
26	2015	6	30	30062015	Landsat-8	5,338,000	356	2018	6	28	28062018	Sentinel-2	122,200
27	2015	6	30	30062015	Landsat-8	169,200	357	2018	6	28	28062018	Sentinel-2	6324
28	2015	6	30	30062015	Landsat-8	15,230	358	2018	7	1	1072018	Sentinel-2	6329
29	2015	6	30	30062015	Landsat-8	22,040	359	2018	7	3	3072018	Sentinel-2	878,000
30	2015	6	30	30062015	Landsat-8	96,980	360	2018	7	3	3072018	Sentinel-2	65,790
31	2015	6	30	30062015	Landsat-8	1,430,000	361	2018	7	6	6072018	Sentinel-2	2,348,000
32	2015	6	30	30062015	Landsat-8	106,900	362	2018	7	8	8072018	Sentinel-2	305,300
33	2015	6	30	30062015	Landsat-8	31,680	363	2018	7	8	8072018	Sentinel-2	534,800
34	2015	6	30	30062015	Landsat-8	5,050,000	364	2018	7	8	8072018	Sentinel-2	15,860
35	2015	6	30	30062015	Landsat-8	37,950,000	365	2018	7	13	13072018	Sentinel-2	150,700
36	2015	6	30	30062015	Landsat-8	774,700	366	2018	7	13	13072018	Sentinel-2	37,080
37	2015	7	16	16072015	Landsat-8	20,260,000	367	2018	7	13	13072018	Sentinel-2	80,570
38	2015	7	16	16072015	Landsat-8	31,120	368	2018	7	13	13072018	Sentinel-2	7072
39	2015	7	16	16072015	Landsat-8	201,900	369	2018	7	13	13072018	Sentinel-2	18,240
40	2015	7	16	16072015	Landsat-8	17,850	370	2018	7	16	16072018	Sentinel-2	14,810
41	2015	7	16	16072015	Landsat-8	5852	371	2018	7	18	18072018	Sentinel-2	30,930
42	2015	7	16	16072015	Landsat-8	5,139,000	372	2018	7	18	18072018	Sentinel-2	14,110
43	2015	8	17	17082015	Landsat-8	5,744	373	2018	7	18	18072018	Sentinel-2	24,300
44	2015	8	17	17082015	Landsat-8	570,000	374	2018	7	18	18072018	Sentinel-2	32,030
45	2015	8	17	17082015	Landsat-8	29,520	375	2018	7	21	21072018	Sentinel-2	2570
46	2015	8	17	17082015	Landsat-8	425,100	376	2018	7	21	21072018	Sentinel-2	18,520
47	2015	8	17	17082015	Landsat-8	14,340	377	2018	7	23	23072018	Sentinel-2	12,020
48	2015	8	17	17082015	Landsat-8	30,870	378	2018	7	28	28072018	Sentinel-2	22,140
49	2015	8	17	17082015	Landsat-8	22,340	379	2018	8	2	2082018	Sentinel-2	18,320
50	2015	8	17	17082015	Landsat-8	85,680	380	2018	8	2	2082018	Sentinel-2	20,130
51	2015	8	17	17082015	Landsat-8	81,850	381	2018	8	2	2082018	Sentinel-2	1439
52	2015	8	17	17082015	Landsat-8	10,690,000	382	2018	8	2	2082018	Sentinel-2	16,770
53	2015	8	17	17082015	Landsat-8	163,600	383	2018	8	2	2082018	Sentinel-2	30,940
54	2015	8	17	17082015	Landsat-8	1,174,000	384	2018	8	7	7082018	Sentinel-2	329,800
55	2015	8	17	17082015	Landsat-8	32,340	385	2018	8	7	7082018	Sentinel-2	73,950
56	2015	8	17	17082015	Landsat-8	504,100	386	2018	8	12	12082018	Sentinel-2	31,160
57	2015	8	17	17082015	Landsat-8	18,910	387	2018	8	15	15082018	Sentinel-2	51,780
58	2015	8	17	17082015	Landsat-8	15,570	388	2018	8	15	15082018	Sentinel-2	186,900
59	2015	8	17	17082015	Landsat-8	6939	389	2018	8	17	17082018	Sentinel-2	70,270
60	2015	8	17	17082015	Landsat-8	1,029,000	390	2018	8	17	17082018	Sentinel-2	1312
61	2015	8	17	17082015	Landsat-8	40,340	391	2018	8	17	17082018	Sentinel-2	13,390
62	2015	8	21	21082015	Sentinel-2	1,231,000	392	2018	8	22	22082018	Sentinel-2	43,870
63	2015	8	21	21082015	Sentinel-2	57,210	393	2018	8	22	22082018	Sentinel-2	47,230
64	2015	9	2	2092015	Landsat-8	473,800	394	2018	8	25	25082018	Sentinel-2	710,500
65	2015	9	2	2092015	Landsat-8	66,060	395	2018	8	27	27082018	Sentinel-2	6,754,000
66	2015	9	2	2092015	Landsat-8	71,790	396	2018	9	9	19092018	Sentinel-2	59,990

No.	Year	Month	Day	Date	Imagery	Area (m^2)	No.	Year	Month	Day	Date	Imagery	Area (m^2)
67	2015	9	2	2092015	Landsat-8	373,200	397	2018	9	9	9092018	Sentinel-2	222,100
68	2015	9	2	2092015	Landsat-8	6230	398	2018	9	9	9092018	Sentinel-2	15,700
69	2015	9	2	2092015	Landsat-8	5183	399	2018	9	21	21092018	Sentinel-2	27,820
70	2015	9	2	2092015	Landsat-8	8226	400	2018	9	29	29092018	Sentinel-2	266,400
71	2015	9	2	2092015	Landsat-8	7894	401	2018	10	6	6102018	Sentinel-2	4,619,000
72	2015	9	18	18092015	Landsat-8	176,300	402	2019	4	29	29042019	Sentinel-2	18,330
73	2015	9	18	18092015	Landsat-8	70,460	403	2019	5	7	7052019	Sentinel-2	23,560
74	2015	10	12	12102015	Landsat-7	303,800	404	2019	5	17	17052019	Sentinel-2	8492
75	2015	10	12	12102015	Landsat-7	329,500	405	2019	5	19	19052019	Sentinel-2	5064
76	2016	6	13	13062016	Sentinel-2	554,200	406	2019	5	22	22052019	Sentinel-2	4721
77	2016	6	13	13062016	Sentinel-2	204,500	407	2019	5	22	22052019	Sentinel-2	7206
78	2016	6	13	13062016	Sentinel-2	65,400	408	2019	5	24	24052019	Sentinel-2	5133
79	2016	6	13	13062016	Sentinel-2	92,880	409	2019	5	24	24052019	Sentinel-2	1989
80	2016	6	13	13062016	Sentinel-2	94,020	410	2019	5	24	24052019	Sentinel-2	29,080
81	2016	6	13	13062016	Sentinel-2	93,330	411	2019	5	27	27052019	Sentinel-2	9199
82	2016	6	13	13062016	Sentinel-2	51,230	412	2019	5	27	27052019	Sentinel-2	2695
83	2016	6	13	13062016	Sentinel-2	63,120	413	2019	5	29	29052019	Sentinel-2	37,140
84	2016	6	13	13062016	Sentinel-2	19,170	414	2019	5	29	29052019	Sentinel-2	56,290
85	2016	6	13	13062016	Sentinel-2	51,950	415	2019	5	29	29052019	Sentinel-2	5268
86	2016	6	13	13062016	Sentinel-2	52,380	416	2019	5	29	29052019	Sentinel-2	6547
87	2016	6	13	13062016	Sentinel-2	5987	417	2019	5	29	29052019	Sentinel-2	12,360
88	2016	6	13	13062016	Sentinel-2	4187	418	2019	5	29	29052019	Sentinel-2	12,600
89	2016	6	13	13062016	Sentinel-2	10,980	419	2019	5	29	29052019	Sentinel-2	9172
90	2016	6	13	13062016	Sentinel-2	9773	420	2019	5	29	29052019	Sentinel-2	19,130
91	2016	6	13	13062016	Sentinel-2	18,890	421	2019	5	29	29052019	Sentinel-2	23,230
92	2016	6	13	13062016	Sentinel-2	14,860	422	2019	5	29	29052019	Sentinel-2	10,570
93	2016	6	13	13062016	Sentinel-2	13,040	423	2019	5	29	29052019	Sentinel-2	12,020
94	2016	6	13	13062016	Sentinel-2	35,750	424	2019	5	29	29052019	Sentinel-2	9245
95	2016	6	13	13062016	Sentinel-2	22,730	425	2019	5	29	29052019	Sentinel-2	5655
96	2016	6	13	13062016	Sentinel-2	10,230	426	2019	6	1	1062019	Sentinel-2	5789
97	2016	6	13	13062016	Sentinel-2	2073	427	2019	6	1	1062019	Sentinel-2	9754
98	2016	6	13	13062016	Sentinel-2	6431	428	2019	6	1	1062019	Sentinel-2	9351
99	2016	6	13	13062016	Sentinel-2	6260	429	2019	6	1	1062019	Sentinel-2	3766
100	2016	6	13	13062016	Sentinel-2	9379	430	2019	6	1	1062019	Sentinel-2	5845
101	2016	6	13	13062016	Sentinel-2	5558	431	2019	6	1	1062019	Sentinel-2	5484
102	2016	6	13	13062016	Sentinel-2	20,580	432	2019	6	1	1062019	Sentinel-2	2018
103	2016	6	13	13062016	Sentinel-2	6165	433	2019	6	3	3062019	Sentinel-2	283,100
104	2016	6	13	13062016	Sentinel-2	22,410	434	2019	6	3	3062019	Sentinel-2	5181
105	2016	6	13	13062016	Sentinel-2	17,170	435	2019	6	3	3062019	Sentinel-2	78,140
106	2016	6	13	13062016	Sentinel-2	2872	436	2019	6	3	3062019	Sentinel-2	21,100
107	2016	6	13	13062016	Sentinel-2	17,040	437	2019	6	3	3062019	Sentinel-2	8376
108	2016	6	13	13062016	Sentinel-2	3433	438	2019	6	6	6062019	Sentinel-2	6335
109	2016	6	13	13062016	Sentinel-2	2833	439	2019	6	8	8062019	Sentinel-2	16,510
110	2016	6	26	26062016	Sentinel-2	7,536,000	440	2019	6	8	8062019	Sentinel-2	12,400
111	2016	6	26	26062016	Sentinel-2	1,304,000	441	2019	6	8	8062019	Sentinel-2	37,900
112	2016	6	26	26062016	Sentinel-2	280,800	442	2019	6	8	8062019	Sentinel-2	26,980
113	2016	6	26	26062016	Sentinel-2	488,300	443	2019	6	8	8062019	Sentinel-2	11,840
114	2016	6	26	26062016	Sentinel-2	63,250	444	2019	6	11	11062019	Sentinel-2	52,760
115	2016	6	26	26062016	Sentinel-2	36,640	445	2019	6	11	11072019	Sentinel-2	157,400
116	2016	6	26	26062016	Sentinel-2	91,530	446	2019	6	11	11072019	Sentinel-2	236,700
117	2016	6	26	26062016	Sentinel-2	66,310	447	2019	6	13	13062019	Sentinel-2	303,000
118	2016	6	26	26062016	Sentinel-2	5005	448	2019	6	13	13062019	Sentinel-2	58,870
119	2016	6	26	26062016	Sentinel-2	25,710	449	2019	6	13	13062019	Sentinel-2	15,500
120	2016	6	26	26062016	Sentinel-2	252,400	450	2019	6	13	13062019	Sentinel-2	47,520
121	2016	6	26	26062016	Sentinel-2	29,010	451	2019	6	13	13062019	Sentinel-2	3789
122	2016	7	3	3072016	Sentinel-2	168,200	452	2019	6	13	13062019	Sentinel-2	4943
123	2016	7	3	3072016	Sentinel-2	50,910	453	2019	6	13	13062019	Sentinel-2	17,630
124	2016	7	3	3072016	Sentinel-2	22,700	454	2019	6	13	13062019	Sentinel-2	1962
125	2016	7	3	3072016	Sentinel-2	36,420	455	2019	6	13	13062019	Sentinel-2	4811
126	2016	7	3	3072016	Sentinel-2	21,480	456	2019	6	18	18062019	Sentinel-2	20,380
127	2016	7	3	3072016	Sentinel-2	53,180	457	2019	6	18	18062019	Sentinel-2	45,740
128	2016	7	3	3072016	Sentinel-2	48,910	458	2019	6	18	18062019	Sentinel-2	15,340
129	2016	7	3	3072016	Sentinel-2	45,660	459	2019	6	18	18062019	Sentinel-2	9706
130	2016	7	3	3072016	Sentinel-2	21,640	460	2019	6	18	18062019	Sentinel-2	7033
131	2016	7	3	3072016	Sentinel-2	328,700	461	2019	6	18	18062019	Sentinel-2	7621

No.	Year	Month	Day	Date	Imagery	Area (m^2)	No.	Year	Month	Day	Date	Imagery	Area (m^2)
132	2016	7	3	3072016	Sentinel-2	315,300	462	2019	6	18	18062019	Sentinel-2	2,261,000
133	2016	7	3	3072016	Sentinel-2	114,600	463	2019	6	18	18062019	Sentinel-2	188,600
134	2016	7	3	3072016	Sentinel-2	8185	464	2019	6	23	23062019	Sentinel-2	169,300
135	2016	7	3	3072016	Sentinel-2	16,380	465	2019	6	23	23062019	Sentinel-2	193,200
136	2016	7	3	3072016	Sentinel-2	13,850	466	2019	6	23	23062019	Sentinel-2	827,800
137	2016	7	3	3072016	Sentinel-2	17,550	467	2019	6	23	23062019	Sentinel-2	33,610
138	2016	7	3	3072016	Sentinel-2	30,480	468	2019	6	23	23062019	Sentinel-2	9397
139	2016	7	3	3072016	Sentinel-2	20,500	469	2019	6	28	28062019	Sentinel-2	20,640
140	2016	7	3	3072016	Sentinel-2	7337	470	2019	6	28	28062019	Sentinel-2	11,670
141	2016	7	3	3072016	Sentinel-2	12,400	471	2019	6	28	28062019	Sentinel-2	400,700
142	2016	7	3	3072016	Sentinel-2	7921	472	2019	6	28	28062019	Sentinel-2	31,680
143	2016	7	3	3072016	Sentinel-2	4858	473	2019	6	28	28062019	Sentinel-2	2599
144	2016	7	3	3072016	Sentinel-2	13,790	474	2019	6	28	28062019	Sentinel-2	39,200
145	2016	7	3	3072016	Sentinel-2	5691	475	2019	7	1	1072019	Sentinel-2	5961
146	2016	7	3	3072016	Sentinel-2	2234	476	2019	7	1	1072019	Sentinel-2	5371
147	2016	7	3	3072016	Sentinel-2	9517	477	2019	7	3	3072019	Sentinel-2	68,200
148	2016	7	3	3072016	Sentinel-2	27,420	478	2019	7	3	3072019	Sentinel-2	12,410
149	2016	7	16	16072016	Sentinel-2	10,580,000	479	2019	7	3	3072019	Sentinel-2	127,800
150	2016	7	16	16072016	Sentinel-2	294,700	480	2019	7	3	3072019	Sentinel-2	83,930
151	2016	7	16	16072016	Sentinel-2	1,651,000	481	2019	7	3	3072019	Sentinel-2	33,420
152	2016	7	16	16072016	Sentinel-2	8215	482	2019	7	3	3072019	Sentinel-2	4297
153	2016	7	16	16072016	Sentinel-2	2,646,000	483	2019	7	3	3072019	Sentinel-2	29,800
154	2016	7	16	16072016	Sentinel-2	6052	484	2019	7	3	3072019	Sentinel-2	10,410
155	2016	7	16	16072016	Sentinel-2	36,440	485	2019	7	6	6072019	Sentinel-2	3221
156	2016	7	16	16072016	Sentinel-2	17,340	486	2019	7	8	8072019	Sentinel-2	31,720
157	2016	7	16	16072016	Sentinel-2	7591	487	2019	7	8	8072019	Sentinel-2	7330
158	2016	7	16	16072016	Sentinel-2	113,500	488	2019	7	8	8072019	Sentinel-2	605,900
159	2016	7	16	16072016	Sentinel-2	10,480	489	2019	7	8	8072019	Sentinel-2	5203
160	2016	7	16	16072016	Sentinel-2	5788	490	2019	7	8	8072019	Sentinel-2	15,210
161	2016	7	16	16072016	Sentinel-2	6107	491	2019	7	8	8072019	Sentinel-2	17,080
162	2016	7	16	16072016	Sentinel-2	2623	492	2019	7	13	13072019	Sentinel-2	11,430
163	2016	7	16	16072016	Sentinel-2	11,340	493	2019	7	13	13072019	Sentinel-2	26,720
164	2016	7	16	16072016	Sentinel-2	24,420	494	2019	7	14	14052019	Sentinel-2	10,360
165	2016	7	16	16072016	Sentinel-2	1178	495	2019	7	16	16072019	Sentinel-2	84,870
166	2016	7	16	16072016	Sentinel-2	14,990	496	2019	7	16	16072019	Sentinel-2	56,510
167	2016	7	16	16072016	Sentinel-2	15,330	497	2019	7	18	18072019	Sentinel-2	6161
168	2016	7	16	16072016	Sentinel-2	348,700	498	2019	7	23	23072019	Sentinel-2	13,120
169	2016	7	16	16072016	Sentinel-2	16,630	499	2019	7	23	23072019	Sentinel-2	15,820
170	2016	7	16	16072016	Sentinel-2	6034	500	2019	7	23	23072019	Sentinel-2	32,250
171	2016	7	16	16072016	Sentinel-2	3501	501	2019	7	28	28072019	Sentinel-2	65,860
172	2016	7	16	16072016	Sentinel-2	7033	502	2019	7	28	28072019	Sentinel-2	60,370
173	2016	7	16	16072016	Sentinel-2	6112	503	2019	7	31	31072019	Sentinel-2	10,880,000
174	2016	7	16	16072016	Sentinel-2	1992	504	2019	7	31	31072019	Sentinel-2	150,400
175	2016	7	16	16072016	Sentinel-2	854.9	505	2019	7	31	31072019	Sentinel-2	60,240
176	2016	7	16	16072016	Sentinel-2	243,100	506	2019	7	31	31072019	Sentinel-2	2749
177	2016	7	23	23072016	Sentinel-2	79,710	507	2019	8	5	5082019	Sentinel-2	9158
178	2016	7	23	23072016	Sentinel-2	5622	508	2019	8	7	7082019	Sentinel-2	530,800
179	2016	7	23	23072016	Sentinel-2	4053	509	2019	8	7	7082019	Sentinel-2	266,100
180	2016	7	23	23072016	Sentinel-2	15,120	510	2019	8	7	7082019	Sentinel-2	13,530,000
181	2016	7	23	23072016	Sentinel-2	5374	511	2019	8	7	7082019	Sentinel-2	105,500
182	2016	7	23	23072016	Sentinel-2	386.8	512	2019	8	17	17082019	Sentinel-2	1,737,000
183	2016	7	23	23072016	Sentinel-2	479.5	513	2019	8	17	17082019	Sentinel-2	95,000
184	2016	7	23	23072016	Sentinel-2	3878	514	2019	8	17	17082019	Sentinel-2	289,000
185	2016	7	23	23072016	Sentinel-2	3388	515	2019	8	17	17082019	Sentinel-2	34,110
186	2016	7	23	23072016	Sentinel-2	11,770	516	2019	8	20	20082019	Sentinel-2	57,440
187	2016	7	23	23072016	Sentinel-2	1466	517	2019	8	22	22082019	Sentinel-2	61,490
188	2016	7	23	23072016	Sentinel-2	1515	518	2019	8	22	22082019	Sentinel-2	3327
189	2016	7	23	23072016	Sentinel-2	3239	519	2019	8	30	30082019	Sentinel-2	8,957,000
190	2016	7	23	23072016	Sentinel-2	388,900	520	2019	8	30	30082019	Sentinel-2	23,200
191	2016	7	23	23072016	Sentinel-2	9926	521	2019	9	1	1092019	Sentinel-2	2,280,000
192	2016	7	23	23072016	Sentinel-2	3390	522	2019	9	1	1092019	Sentinel-2	1,438,000
193	2016	7	23	23072016	Sentinel-2	219,500	523	2019	9	1	1092019	Sentinel-2	9084
194	2016	7	23	23072016	Sentinel-2	8915	524	2019	9	1	1092019	Sentinel-2	150,700
195	2016	7	23	23072016	Sentinel-2	52,410	525	2019	9	1	1092019	Sentinel-2	2,810,000
196	2016	7	23	23072016	Sentinel-2	39,210	526	2019	9	1	1092019	Sentinel-2	44,940
197	2016	7	23	23072016	Sentinel-2	19,710	527	2019	9	1	1092019	Sentinel-2	26,510
198	2016	7	23	23072016	Sentinel-2	25,620	528	2019	9	1	1092019	Sentinel-2	2835
199	2016	7	23	23072016	Sentinel-2	18,450	529	2019	9	1	1092019	Sentinel-2	106,400

No.	Year	Month	Day	Date	Imagery	Area (m^2)	No.	Year	Month	Day	Date	Imagery	Area (m^2)
200	2016	7	23	23072016	Sentinel-2	67,460	530	2019	9	1	1092019	Sentinel-2	7332
201	2016	7	23	23072016	Sentinel-2	4843	531	2019	9	6	6092019	Sentinel-2	12,650
202	2016	7	23	23072016	Sentinel-2	97,420	532	2019	9	6	6092019	Sentinel-2	179,500
203	2016	7	23	23072016	Sentinel-2	23,450	533	2019	9	6	6092019	Sentinel-2	12,040
204	2016	7	23	23072016	Sentinel-2	20,230	534	2019	9	6	6092019	Sentinel-2	67,160
205	2016	7	23	23072016	Sentinel-2	5118	535	2019	9	11	11092019	Sentinel-2	1,058,000
206	2016	7	23	23072016	Sentinel-2	2605	536	2019	9	21	21092019	Sentinel-2	64,710
207	2016	7	26	26072016	Sentinel-2	88,380	537	2019	9	24	24092019	Sentinel-2	27,290
208	2016	7	26	26072016	Sentinel-2	22,470	538	2019	9	24	24092019	Sentinel-2	44,440
209	2016	7	26	26072016	Sentinel-2	6720	539	2019	10	4	4102019	Sentinel-2	13,200
210	2016	7	26	26072016	Sentinel-2	11,980	540	2019	10	6	6102019	Sentinel-2	62,150
211	2016	7	26	26072016	Sentinel-2	4417	541	2019	10	6	6102019	Sentinel-2	70,370
212	2016	7	26	26072016	Sentinel-2	7437	542	2019	10	6	6102019	Sentinel-2	48,690
213	2016	7	26	26072016	Sentinel-2	11,370	543	2019	10	6	6102019	Sentinel-2	24,760
214	2016	8	26	6072016	Sentinel-2	8876	544	2019	10	6	6102019	Sentinel-2	10,610
215	2016	8	5	5082016	Sentinel-2	13,670	545	2019	10	6	6102019	Sentinel-2	18,430
216	2016	8	5	5082016	Sentinel-2	31,270	546	2019	10	6	6102019	Sentinel-2	93,260
217	2016	8	5	5082016	Sentinel-2	10,000	547	2019	10	11	11102019	Sentinel-2	51,390
218	2016	8	5	5082016	Sentinel-2	18,930	548	2019	10	11	11102019	Sentinel-2	69,020
219	2016	8	5	5082016	Sentinel-2	26,190	549	2019	10	16	16102019	Sentinel-2	317,100
220	2016	8	12	12082016	Sentinel-2	6405	550	2019	10	16	16102019	Sentinel-2	22,580
221	2016	8	12	12082016	Sentinel-2	4811	551	2020	4	21	21042020	Sentinel-2	21,670
222	2016	8	12	12082016	Sentinel-2	22,930	552	2020	5	1	1052020	Sentinel-2	121,700
223	2016	8	12	12082016	Sentinel-2	24,830	553	2020	5	1	1052020	Sentinel-2	19,810
224	2016	8	12	12082016	Sentinel-2	63,220	554	2020	5	13	13052020	Sentinel-2	19,930
225	2016	8	12	12082016	Sentinel-2	10,610	555	2020	5	23	23052020	Sentinel-2	887,700
226	2016	8	12	12082016	Sentinel-2	24,650	556	2020	5	23	23052020	Sentinel-2	23,840
227	2016	8	12	12082016	Sentinel-2	15,390	557	2020	5	31	31052020	Sentinel-2	1,312,000
228	2016	8	15	15082016	Sentinel-2	75,710	558	2020	5	31	31052020	Sentinel-2	2,885,000
229	2016	8	15	15082016	Sentinel-2	18,650	559	2020	5	31	31052020	Sentinel-2	91,550
230	2016	8	25	25082016	Sentinel-2	75,080	560	2020	5	31	31052020	Sentinel-2	15,290
231	2016	8	25	25082016	Sentinel-2	30,690	561	2020	6	2	2062020	Sentinel-2	26,690
232	2016	8	25	25082016	Sentinel-2	18,470	562	2020	6	2	2062020	Sentinel-2	115,600
233	2016	8	25	25082016	Sentinel-2	25,320	563	2020	6	2	2062020	Sentinel-2	61,700
234	2016	8	25	25082016	Sentinel-2	4354	564	2020	6	2	2062020	Sentinel-2	26,580
235	2016	8	25	25082016	Sentinel-2	4900	565	2020	6	2	2062020	Sentinel-2	8253
236	2016	8	25	25082016	Sentinel-2	42,380	566	2020	6	2	2062020	Sentinel-2	101,300
237	2016	9	1	1092016	Sentinel-2	2,469,000	567	2020	6	5	5062020	Sentinel-2	161,800
238	2016	9	1	1092016	Sentinel-2	12,790,000	568	2020	6	5	5062020	Sentinel-2	10,270
239	2016	9	1	1092016	Sentinel-2	32,740	569	2020	6	5	5062020	Sentinel-2	46,650
240	2016	9	1	1092016	Sentinel-2	227,100	570	2020	6	5	5062020	Sentinel-2	78,100
241	2016	9	1	1092016	Sentinel-2	40,910	571	2020	6	5	5062020	Sentinel-2	13,910
242	2016	9	1	1092016	Sentinel-2	22,590	572	2020	6	7	7062020	Sentinel-2	12,770
243	2016	9	1	1092016	Sentinel-2	11,440	573	2020	6	7	7062020	Sentinel-2	7744
244	2017	5	9	9052017	Sentinel-2	18,140	574	2020	6	7	7062020	Sentinel-2	2224
245	2017	5	9	9052017	Sentinel-2	1764	575	2020	6	7	7062020	Sentinel-2	39,130
246	2017	5	9	9052017	Sentinel-2	6671	576	2020	6	7	7062020	Sentinel-2	101,400
247	2017	5	9	9052017	Sentinel-2	23,640	577	2020	6	7	7062020	Sentinel-2	2534
248	2017	5	9	9052017	Sentinel-2	9006	578	2020	6	7	7062020	Sentinel-2	38,610
249	2017	5	9	9052017	Sentinel-2	7851	579	2020	6	7	7062020	Sentinel-2	13,470
250	2017	5	12	12052017	Sentinel-2	27,370	580	2020	6	7	7062020	Sentinel-2	38,620
251	2017	5	22	22052017	Sentinel-2	60,670	581	2020	6	7	7062020	Sentinel-2	3642
252	2017	5	22	22052017	Sentinel-2	50,050	582	2020	6	7	7062020	Sentinel-2	5200
253	2017	5	22	22052017	Sentinel-2	83,490	583	2020	6	7	7062020	Sentinel-2	5954
254	2017	5	22	22052017	Sentinel-2	18,550	584	2020	6	10	10062020	Sentinel-2	132,800
255	2017	5	22	22052017	Sentinel-2	16,510	585	2020	6	12	12062020	Sentinel-2	35,480
256	2017	5	22	22052017	Sentinel-2	1706	586	2020	6	12	12062020	Sentinel-2	216,000
257	2017	5	22	22052017	Sentinel-2	32,730	587	2020	6	12	12062020	Sentinel-2	36,830
258	2017	5	22	22052017	Sentinel-2	205,600	588	2020	6	12	12062020	Sentinel-2	13,670
259	2017	5	22	22052017	Sentinel-2	5801	589	2020	6	12	12062020	Sentinel-2	116,800
260	2017	5	22	22052017	Sentinel-2	34,290	590	2020	6	12	12062020	Sentinel-2	20,480
261	2017	5	22	22052017	Sentinel-2	26,930	591	2020	6	17	17062020	Sentinel-2	262,300
262	2017	5	29	29052017	Sentinel-2	12,960	592	2020	6	17	17062020	Sentinel-2	27,250
263	2017	5	29	29052017	Sentinel-2	51,440	593	2020	6	17	17062020	Sentinel-2	58,620
264	2017	5	29	29052017	Sentinel-2	42,960	594	2020	6	22	22062020	Sentinel-2	38,590

No.	Year	Month	Day	Date	Imagery	Area (m^2)	No.	Year	Month	Day	Date	Imagery	Area (m^2)
265	2017	5	29	29052017	Sentinel-2	73,730	595	2020	6	22	22062020	Sentinel-2	12,970
266	2017	5	29	29052017	Sentinel-2	4667	596	2020	6	25	25062020	Sentinel-2	642,900
267	2017	5	29	29052017	Sentinel-2	2779	597	2020	6	25	25062020	Sentinel-2	7354
268	2017	5	29	29052017	Sentinel-2	5866	598	2020	6	25	25062020	Sentinel-2	569,400
269	2017	5	29	29052017	Sentinel-2	20,300	599	2020	6	27	27062020	Sentinel-2	381,700
270	2017	5	29	29052017	Sentinel-2	5799	600	2020	6	27	27062020	Sentinel-2	122,400
271	2017	5	29	29052017	Sentinel-2	16,910	601	2020	6	27	27062020	Sentinel-2	9,103,000
272	2017	5	29	29052017	Sentinel-2	5432	602	2020	6	27	27062020	Sentinel-2	7893
273	2017	5	29	29052017	Sentinel-2	4607	603	2020	6	27	27062020	Sentinel-2	4949
274	2017	5	29	29052017	Sentinel-2	49,690	604	2020	6	27	27062020	Sentinel-2	11,370
275	2017	6	1	1062017	Sentinel-2	1,105,000	605	2020	6	27	27062020	Sentinel-2	3730
276	2017	6	11	11062017	Sentinel-2	76,350	606	2020	6	30	30062020	Sentinel-2	17,380
277	2017	6	11	11062017	Sentinel-2	12,840	607	2020	6	30	30062020	Sentinel-2	8559
278	2017	7	1	1072017	Sentinel-2	169,000	608	2020	7	2	2072020	Sentinel-2	1,105,000
279	2017	7	1	1072017	Sentinel-2	293,00	609	2020	7	2	2072020	Sentinel-2	6,691,000
280	2017	7	1	1072017	Sentinel-2	440,600	610	2020	7	2	2072020	Sentinel-2	33,270
281	2017	7	1	1072017	Sentinel-2	2,732,000	611	2020	7	2	2072020	Sentinel-2	1,209,000
282	2017	7	1	1072017	Sentinel-2	11,550	612	2020	7	2	2072020	Sentinel-2	55,370
283	2017	7	1	1072017	Sentinel-2	8572	613	2020	7	2	2072020	Sentinel-2	49,600
284	2017	7	1	1072017	Sentinel-2	6875	614	2020	7	2	2072020	Sentinel-2	24,310
285	2017	7	1	1072017	Sentinel-2	17,300	615	2020	7	2	2072020	Sentinel-2	89,960
286	2017	7	3	3072017	Sentinel-2	54,790	616	2020	7	2	2072020	Sentinel-2	19,590
287	2017	7	3	3072017	Sentinel-2	16,890	617	2020	7	2	2072020	Sentinel-2	6726
288	2017	7	6	6072017	Sentinel-2	497,600	618	2020	7	5	5072020	Sentinel-2	61,330
289	2017	7	11	11072017	Sentinel-2	134,100	619	2020	7	5	5072020	Sentinel-2	328,500
290	2017	7	11	11072017	Sentinel-2	918,300	620	2020	7	31	31072018	Sentinel-2	7608
291	2017	7	11	11072017	Sentinel-2	18,570	621	2020	7	7	7072020	Sentinel-2	4874
292	2017	7	11	11072017	Sentinel-2	6539	622	2020	7	7	7072020	Sentinel-2	18,690
293	2017	7	11	11072017	Sentinel-2	14,830	623	2020	7	7	7072020	Sentinel-2	19,190
294	2017	7	23	23072017	Sentinel-2	172,600	624	2020	7	7	7072020	Sentinel-2	3615
295	2017	7	23	23072017	Sentinel-2	31,660	625	2020	7	7	7072020	Sentinel-2	108,600
296	2017	7	23	23072017	Sentinel-2	169,000	626	2020	7	7	7072020	Sentinel-2	10,350
297	2017	7	23	23072017	Sentinel-2	2053	627	2020	7	12	12072020	Sentinel-2	20,180
298	2017	7	23	23072017	Sentinel-2	10,480	628	2020	7	15	15072020	Sentinel-2	230,700
299	2017	7	23	23072017	Sentinel-2	10,980,000	629	2020	7	15	15072020	Sentinel-2	13,790
300	2017	7	23	23072017	Sentinel-2	5,090,000	630	2020	7	15	15072020	Sentinel-2	897,900
301	2017	7	23	23072017	Sentinel-2	180,800	631	2020	7	15	15072020	Sentinel-2	1,517,000
302	2017	7	28	28072017	Sentinel-2	27,240	632	2020	7	17	17072020	Sentinel-2	1,579,000
303	2017	7	28	28072017	Sentinel-2	400,900	633	2020	7	17	17072020	Sentinel-2	929,500
304	2017	7	28	28072017	Sentinel-2	187,700	634	2020	7	17	17072020	Sentinel-2	126,200
305	2017	8	12	12082017	Sentinel-2	213,800	635	2020	7	17	17072020	Sentinel-2	2,455,000
306	2017	8	12	12082017	Sentinel-2	451,400	636	2020	7	22	22072020	Sentinel-2	1,013,000
307	2017	8	12	12082017	Sentinel-2	17,280	637	2020	7	22	22072020	Sentinel-2	453,700
308	2017	8	12	12082017	Sentinel-2	4320	638	2020	7	22	22072020	Sentinel-2	2,366,000
309	2017	8	12	12082017	Sentinel-2	50,260	639	2020	7	27	27072020	Sentinel-2	73,270
310	2017	8	12	12082017	Sentinel-2	37,790	640	2020	7	27	27072020	Sentinel-2	1,127,000
311	2017	8	12	12082017	Sentinel-2	187,400	641	2020	7	30	30072020	Sentinel-2	416,600
312	2017	8	12	12082017	Sentinel-2	786,300	642	2020	8	1	1082020	Sentinel-2	4773
313	2017	8	12	12082017	Sentinel-2	30,950	643	2020	8	6	6082020	Sentinel-2	3468
314	2017	8	12	12082017	Sentinel-2	4952	644	2020	8	6	6082020	Sentinel-2	59,090
315	2017	8	20	20082017	Sentinel-2	74,950	645	2020	8	11	11082020	Sentinel-2	3476
316	2017	8	20	20082017	Sentinel-2	23,410	646	2020	8	11	11082020	Sentinel-2	178,900
317	2017	8	20	20082017	Sentinel-2	10,850	647	2020	8	11	11082020	Sentinel-2	568,300
318	2017	9	1	1092017	Sentinel-2	688,400	648	2020	8	11	11082020	Sentinel-2	9427
319	2017	9	1	1092017	Sentinel-2	110,500	649	2020	8	11	11082020	Sentinel-2	17,940
320	2017	9	1	1092017	Sentinel-2	23,360	650	2020	8	11	11082020	Sentinel-2	91,750
321	2017	9	6	6092017	Sentinel-2	2,563,000	651	2020	8	11	11082020	Sentinel-2	70,120
322	2017	9	24	24092017	Sentinel-2	25,980	652	2020	8	14	14082020	Sentinel-2	22,120
323	2017	9	24	24092017	Sentinel-2	11,490	653	2020	8	16	16082020	Sentinel-2	342,500
324	2017	9	26	26072017	Sentinel-2	26,630	654	2020	8	16	16082020	Sentinel-2	196,800
325	2017	9	26	26092017	Sentinel-2	26,070	655	2020	8	19	19082020	Sentinel-2	45,260
326	2017	9	26	26092017	Sentinel-2	57,440	656	2020	8	21	21082020	Sentinel-2	59,790
327	2017	9	26	26092017	Sentinel-2	151,800	657	2020	8	26	26082020	Sentinel-2	533,100
328	2017	9	26	26092017	Sentinel-2	47,720	658	2020	8	31	31082020	Sentinel-2	95,980
329	2017	9	26	26092017	Sentinel-2	1555	659	2020	9	15	15092020	Sentinel-2	2,568,000
330	2017	9	26	26092017	Sentinel-2	20,590	660	2020	9	15	15092020	Sentinel-2	76,720

Appendix C The Range of Estimation for Each Factor by Logistic Regression Results of Training Dataset for Each Group

Factor	Group1	Group2	Group3	Group4	Group5	Group6	Group7
Intercept	−86.1	−118.0	−125.0	−160.000	−162.0	−171.0	−160
Slope	0.031	0.034	0.025	0.025	0.026	0.027	0.0264
Aspect -N	0.106	0.094	0.171	0.149	0.143	0.149	0.149
Aspect -NE	0.080	0.092	0.125	0.119	0.102	0.117	0.119
Aspect -E	−0.106	−0.093	−0.050	−0.050	−0.065	−0.053	−0.0502
Aspect -SE	−0.146	−0.138	−0.127	−0.118	−0.115	−0.116	−0.116
Aspect -S	−0.017	−0.009	−0.084	−0.065	−0.056	−0.061	−0.0658
Aspect -SW	0.026	0.029	−0.066	−0.054	−0.050	−0.052	−0.0557
Aspect -W	0.124	0.110	0.069	0.066	0.076	0.064	0.0659
Aspect -NW	−0.073	−0.089	−0.042	−0.051	−0.038	−0.051	−0.0487
Elevation	0.002	0.002	0.002	0.002	0.002	0.002	0.00193
Precipitation	0.006	0.010	0.026	0.027	0.016	0.021	0.0268
Distance to Road	0.000	0.000	0.000	0.000	0.000	0.000	−0.00036
Distance to Settlements	0.001	0.001	0.001	0.001	0.001	0.001	0.000581
LULC1-Open Shrub	57.300	73.400	115.000	122.000	95.100	110.000	122
LULC2-Grassland	58.100	74.100	116.000	122.000	95.800	111.000	122
LULC4-Cropland	58.200	74.300	116.000	122.000	96.000	111.000	122
LULC5-Urban Area	57.500	73.500	116.000	122.000	95.600	110.000	122
LULC6-Barren	47.200	63.200	105.000	111.000	84.700	99.400	111
Annual Air Temperature	−0.316	0.000	−1.700	−0.922	0.156	−0.166	−0.909
Wind Speed	9.500	10.800	19.400	18.900	13.800	16.100	18.8
NDVI	−2.110	−1.800	−2.440	−2.200	−2.360	−2.230	−2.22
Distance to streams	−0.001	−0.002	0.000	−0.002	−0.002	−0.002	−0.00182
Geology-Flood Plain	/	/	1.850	1.810	1.700	1.800	1.81
Geology-Slope	/	/	−0.295	−0.313	−0.290	−0.326	−0.315
Geology-Polygenetic	/	/	−0.595	−0.606	−0.586	−0.596	−0.607
Geology-Mukdadiyah	/	/	−0.164	−0.232	−0.295	−0.257	−0.231
Geology-Injana	/	/	0.806	0.747	0.716	0.742	0.748
Geology-Fatha	/	/	0.961	0.991	1.010	0.985	0.992
Geology-Pilaspi	/	/	0.571	0.595	0.566	0.582	0.594
Geology-Gercus	/	/	0.042	0.070	0.090	0.084	0.069
Geology-Khurmala and Sinjar	/	/	−0.138	−0.109	−0.052	−0.074	−0.11
Geology-Kolosh	/	/	−0.434	−0.365	−0.314	−0.339	−0.363
Geology-Tanjero, Aqra, and Bekhme	/	/	−2.610	−2.590	−2.550	−2.610	−2.59
TWI	/	0.010	0.012	/	0.012	0.012	0.012
Relative Humidity	/	0.102	−0.890	−0.517	0.248	/	−0.51
Distance to Farmland	/	0.000	0.0002	0.004	/	0.00013	0.000149
TPI	/	0.004	/	0.0043	0.004	0.004	0.00426

Appendix D The Range of Estimation for Each Factor by Logistic Regression Results of Validation Dataset for Each Group

Factor	Group1	Group2	Group3	Group4	Group5	Group6	Group7
Intercept	−305	−22.31	104.5	11.36	−142	−371.2	8.71
Slope	0.02825	0.03329	0.02862	0.02837	0.02904	0.03551	0.03116
Aspect-N	0.3124	0.2489	0.2423	0.2105	0.222	0.2304	0.2112
Aspect-NE	0.06258	0.001159	−0.05362	−0.05304	−0.05112	0.01329	−0.05428
Aspect-E	−0.4681	−0.4903	−0.5028	−0.5033	−0.5134	−0.481	−0.506
Aspect-SE	−0.1643	−0.1617	−0.1732	−0.1629	−0.1421	−0.1555	−0.1593
Aspect-S	0.1507	0.2201	0.2219	0.2596	0.2413	0.2304	0.2552
Aspect-SW	0.1	0.1835	0.187	0.2197	0.1928	0.1802	0.2158
Aspect-W	0.01248	−0.00756	0.03013	0.01171	0.02498	−0.00135	0.01194
Aspect-NW	−0.01185	0.00039	0.04304	0.01228	0.02091	−0.02414	0.01988
Elevation	0.00023	0.000224	0.001738	0.000562	0.000136	−0.00099	0.000541
Precipitation	0.1367	0.2364	0.2615	0.2539	0.1956	0.1615	0.2537
Distance to Road	−0.00028	−0.00048	−0.0005856	−0.00062	−0.0006	−0.00044	−0.00062
Distance to Settlements	0.000117	-4.3×10^{-5}	4.081×10^{-5}	4.77×10^{-5}	0.000187	9.28×10^{-5}	4.66×10^{-5}

Factor	Group1	Group2	Group3	Group4	Group5	Group6	Group7
LULC1-Open Shrub	10.65	9.839	9.451	9.454	9.966	10.41	9.5
LULC2-Grassland	11.58	10.73	10.33	10.36	10.8	11.38	10.41
LULC4-Cropland	11.34	10.46	9.966	9.995	10.39	11.12	10.04
LULC5-Urban Area	12.03	11.93	11.71	11.73	11.56	12.33	11.78
LULC6-Barren	1.405	1.33	1.435	1.353	1.237	1.837	1.387
Annual Air Temperature	−0.3361	−11.91	−16.66	−13.64	−7.492	0.6016	−13.58
Wind Speed	73.28	137.2	157.9	149.9	117.1	84.91	149.9
NDVI	−3.157	−2.026	−2.708	−2.052	−2.248	−2.108	−2.069
Distance to streams	0.001483	−0.00143	0.000881	−0.00194	−0.00169	−0.0019	−0.00157
Geology-Flood Plain	/	/	−0.2976	−0.4112	−0.7447	−0.4617	−0.4108
Geology-Slope	/	/	−0.8035	−0.9317	−1.242	−1.355	−0.9299
Geology-Polygenetic	/	/	1.521	1.513	2.038	1.638	1.501
Geology-Mukdadiyah	/	/	1.687	1.493	0.9022	1.117	1.498
Geology-Injana	/	/	−0.3107	−0.4829	−0.6287	−0.4022	−0.479
Geology-Fatha	/	/	0.443	0.4752	0.4789	0.4702	0.4813
Geology-Pilaspi	/	/	−0.7157	−0.6053	−0.6636	−0.4154	−0.6063
Geology-Gercus	/	/	−0.9819	−0.8063	−0.8455	−0.3796	−0.8063
Geology-Khurmala and Sinjar	/	/	2.499	2.612	3.026	2.542	2.583
Geology-Kolosh	/	/	−0.7934	−0.5782	−0.7149	−0.2305	−0.5707
Geology-Tanjero, Aqra, and Bekhme	/	/	−2.256	−2.287	−1.617	−2.532	−2.27
TWI	/	0.03229	0.03427	/	0.03874	0.04388	0.03755
Relative Humidity	/	−7.941	−10.84	−9.169	−4.852	/	−9.132
Distance to Farmland	/	0.000445	0.0004533	0.000418	/	0.00021	0.000418
TPI	/	0.006574	/	0.0072	0.008614	0.01052	0.007242

References

1. Ziadé, R.; Abdallah, C.; Baghdadi, N. The effect of forest fire on mass movement in Lebanese mountainous areas. *Int. J. Wildl. Fire* **2014**, *23*, 845–859. [CrossRef]
2. Salar, S.G. Identification of Forest Fire Risk Zones in the Sartak Watershed, Kurdistan Region, Iraq: Gis and Remote Sensing Applications. *Iraqi Bull. Geol. Min.* **2019**, *15*, 105–122.
3. Pourghasemi, H.R.; Gayen, A.; Panahi, M.; Rezaie, F.; Blaschke, T. Multi-hazard probability assessment and mapping in Iran. *Sci. Total Environ.* **2019**, *692*, 556–571. [CrossRef] [PubMed]
4. Pourtaghi, Z.S.; Pourghasemi, H.R.; Rossi, M. Forest fire susceptibility mapping in the Minudasht forests, Golestan province, Iran. *Environ. Earth Sci.* **2015**, *73*, 1515–1533.
5. Kayet, N.; Chakrabarty, A.; Pathak, K.; Sahoo, S.; Dutta, T.; Hatai, B.K. Comparative analysis of multi-criteria probabilistic FR and AHP models for forest fire risk (FFR) mapping in Melghat Tiger Reserve (MTR) forest. *J. For. Res.* **2020**, *31*, 565–579. [CrossRef]
6. Zanini, G.D.; Sbrissia, A.F. Prescribed burning of pastures: A management tool? *Rev. Ciências Agroveterinárias* **2014**, *12*, 94–103.
7. Jahdi, R.; Salis, M.; Darvishsefat, A.A.; Mostafavi, M.A.; Alcasena, F.; Etemad, V.; Lozano, O.; Spano, D. Calibration of FARSITE simulator in northern Iranian forests. *Nat. Hazards Earth Syst. Sci.* **2015**, *15*, 443–459. [CrossRef]
8. Glasa, J.; Halada, L. On elliptical model for forest fire spread modeling and simulation. *Math. Comput. Simul.* **2008**, *78*, 76–88. [CrossRef]
9. Ashiagbor, G.; Oduro, W.; Gyiele, L.; Siaw, D.; Barnes, V.R.; Agbenyega, O.; Twum-Ampofo, K.; Partey, S.; Thevathasan, N.; Gordon, A.; et al. Toward sustainable land resources management with agroforestry: Empirical evidence from the Sunyani west district of Ghana. *Agrofor. Syst.* **2020**, *94*, 527–537. [CrossRef]
10. Esmaeili Sharif, M.; Jalilvand, H.; Amoozad, M.; Jafari, A.; Sayed Mahale, S.M. The effect of ecological factors on fire in Hyrcanian forests (Case study: Forest areas of Neka, Mazandaran, Iran). *J. For. Res. Dev.* **2018**, *4*, 113–129.
11. Sowmya, S.V.; Somashekar, R.K. Application of remote sensing and geographical information system in mapping forest fire risk zone at Bhadra wildlife sanctuary, India. *J. Environ. Biol.* **2010**, *31*, 969. [PubMed]
12. Adab, H.; Kanniah, K.D.; Solaimani, K. Modeling forest fire risk in the northeast of Iran using remote sensing and GIS techniques. *Nat. Hazards* **2013**, *65*, 1723–1743. [CrossRef]
13. Jung, J.; Kim, C.; Jayakumar, S.; Kim, S.; Han, S.; Kim, D.H.; Heo, J. Forest fire risk mapping of Kolli Hills, India, considering subjectivity and inconsistency issues. *Nat. Hazards* **2013**, *65*, 2129–2146. [CrossRef]
14. Amalina, P.; Prasetyo, L.B.; Rushayati, S.B. Forest Fire Vulnerability Mapping in Way Kambas National Park. *Procedia Environ. Sci.* **2016**, *33*, 239–252. [CrossRef]
15. Gigović, L.; Pourghasemi, H.R.; Drobnjak, S.; Bai, S. Testing a new ensemble model based on SVM and random forest in forest fire susceptibility assessment and its mapping in Serbia's Tara National Park. *Forests* **2019**, *10*, 408. [CrossRef]
16. Rasooli, S.B.; Rashidi, S.; Shabanian, N. Fire sensitivity of broadleaf tree species in plantations of Kurdistan, Iran. *J. For. Res.* **2021**, *32*, 1167–1176. [CrossRef]
17. Vadrevu, K.P.; Eaturu, A.; Badarinath, K.V.S. Fire risk evaluation using multicriteria analysis-a case study. *Environ. Monit. Assess.* **2010**, *166*, 223–239. [CrossRef]

18. Santiago, I.T.; Kheladze, N. GIS Wildland fire Hazard Modeling in Georgia. Matra Project Report, Caucasus Environmental NGO Network. 2011. Available online: http://drm.cenn.org/Local_Case_studies/GIS%20Wildland%20Fire%20Hazard%20Modeling%20in%20Georgia1.pdf (accessed on 17 July 2021).
19. Sachdeva, S.; Bhatia, T.; Verma, A.K. GIS-based evolutionary optimized Gradient Boosted Decision Trees for forest fire susceptibility mapping. *Nat. Hazards* **2018**, *92*, 1399–1418. [CrossRef]
20. Zhang, G.; Wang, M.; Liu, K. Forest Fire Susceptibility Modeling Using a Convolutional Neural Network for Yunnan Province of China. *Int. J. Disaster Risk Sci.* **2019**, *10*, 386–403. [CrossRef]
21. Moayedi, H.; Mehrabi, M.; Bui, D.T.; Pradhan, B.; Foong, L.K. Fuzzy-metaheuristic ensembles for spatial assessment of forest fire susceptibility. *J. Environ. Manag.* **2020**, *260*, 109867. [CrossRef]
22. Hong, H.; Naghibi, S.A.; Dashtpagerdi, M.M.; Pourghasemi, H.R.; Chen, W. A comparative assessment between linear and quadratic discriminant analyses (LDA-QDA) with frequency ratio and weights-of-evidence models for forest fire susceptibility mapping in China. *Arab. J. Geosci.* **2017**, *10*, 167. [CrossRef]
23. Bui, D.T.; Hoang, N.-D.; Samui, P. Spatial pattern analysis and prediction of forest fire using new machine learning approach of Multivariate Adaptive Regression Splines and Differential Flower Pollination optimization: A case study at Lao Cai province (Viet Nam). *J. Environ. Manag.* **2019**, *237*, 476–487.
24. Stolzenburg, W. *Fire in the Rain Forest*; National Emergency Training Center: Emmitsburg, MD, USA, 2001.
25. Food and Agriculture Organization. Fire Management: Global Assessment 2006. *FAO For. Pap.* **2007**, *151*, 135.
26. Pourghasemi, H.R.; Gayen, A.; Lasaponara, R.; Tiefenbacher, J.P. Application of learning vector quantization and different machine learning techniques to assessing forest fire influence factors and spatial modelling. *Environ. Res.* **2020**, *184*, 109321. [CrossRef] [PubMed]
27. Razavi-Termeh, S.V.; Sadeghi-Niaraki, A.; Choi, S.-M. Ubiquitous GIS-based forest fire susceptibility mapping using artificial intelligence methods. *Remote Sens.* **2020**, *12*, 1689. [CrossRef]
28. Stolle, F.; Chomitz, K.M.; Lambin, E.F.; Tomich, T.P. Human ecological intervention and the role of forest fires in human ecology. *For. Ecol. Manag.* **2003**, *179*, 277–292. [CrossRef]
29. de Alvino-Rayol, F.O.; Rayol, B.P. Effect of fire in weeds of agroforestry system, Pará, Brazil. *Rev. Ciências Agroveterinárias* **2020**, *19*, 1–7. [CrossRef]
30. de Alvino-Rayol, F.O.; Rayol, B.P. Effect of fire in seed banks of agroforestry systems, Pará, Brazil. *Rev. Ciências Agroveterinárias* **2019**, *18*, 489–498. [CrossRef]
31. Minnich, R.A. An integrated model of two fire regimes. *Conserv. Biol.* **2001**, *15*, 1549–1553. [CrossRef]
32. Broncano, M.J.; Retana, J. Topography and pre-fire vegetation affecting the spatial heterogeneity generated after a large forest wildfire in the Mediterranean Basin. *Int. J. Wildl. Fire* **2004**, *13*, 209–216. [CrossRef]
33. Dlamini, W.M. A Bayesian belief network analysis of factors influencing wildfire occurrence in Swaziland. *Environ. Model. Softw.* **2010**, *25*, 199–208. [CrossRef]
34. Pourtaghi, Z.S.; Pourghasemi, H.R.; Aretano, R.; Semeraro, T. Investigation of general indicators influencing on forest fire and its susceptibility modeling using different data mining techniques. *Ecol. Indic.* **2016**, *64*, 72–84. [CrossRef]
35. Ghorbanzadeh, O.; Blaschke, T.; Gholamnia, K.; Aryal, J. Forest fire susceptibility and risk mapping using social/infrastructural vulnerability and environmental variables. *Fire* **2019**, *2*, 50. [CrossRef]
36. Vázquez, A.; Moreno, J.M. Spatial distribution of forest fires in Sierra de Gredos (Central Spain). *For. Ecol. Manag.* **2001**, *147*, 55–65. [CrossRef]
37. Lozano, F.J.; Suárez-Seoane, S.; Kelly, M.; Luis, E. A multi-scale approach for modeling fire occurrence probability using satellite data and classification trees: A case study in a mountainous Mediterranean region. *Remote Sens. Environ.* **2008**, *112*, 708–719. [CrossRef]
38. Zumbrunnen, T.; Pezzatti, G.B.; Menéndez, P.; Bugmann, H.; Bürgi, M.; Conedera, M. Weather and human impacts on forest fires: 100 years of fire history in two climatic regions of Switzerland. *For. Ecol. Manag.* **2011**, *261*, 2188–2199. [CrossRef]
39. Justus, J. A case study in concept determination: Ecological diversity. In *Philosophy of Ecology*; Elsevier: Amsterdam, The Netherlands, 2011; pp. 147–168.
40. Jaiswal, R.K.; Mukherjee, S.; Raju, K.D.; Saxena, R. Forest fire risk zone mapping from satellite imagery and GIS. *Int. J. Appl. Earth Obs. Geoinf.* **2002**, *4*, 1–10. [CrossRef]
41. Dong, X.U.; Li-min, D.A.I.; Guo-fan, S.; Lei, T.; Hui, W. Forest fire risk zone mapping from satellite images and GIS for Baihe Forestry Bureau, Jilin, China. *J. For. Res.* **2005**, *16*, 169–174. [CrossRef]
42. Keane, R.E.; Drury, S.A.; Karau, E.C.; Hessburg, P.F.; Reynolds, K.M. A method for mapping fire hazard and risk across multiple scales and its application in fire management. *Ecol. Modell.* **2010**, *221*, 2–18. [CrossRef]
43. Paz, S.; Carmel, Y.; Jahshan, F.; Shoshany, M. Post-fire analysis of pre-fire mapping of fire-risk: A recent case study from Mt. Carmel (Israel). *For. Ecol. Manag.* **2011**, *262*, 1184–1188. [CrossRef]
44. Eskandari, S.; Ghadikolaei, J.O.; Jalilvand, H.; Saradjian, M.R. Detection of fire high-risk areas in northern forests of Iran using Dong model. *World Appl. Sci. J.* **2013**, *27*, 770–773.
45. Rasooli, S.B.; Bonyad, A.E. Evaluating the efficiency of the Dong model in determining fire vulnerability in Iran's Zagros forests. *J. For. Res.* **2019**, *30*, 1447–1458. [CrossRef]
46. Mahdavi, A. Forests and rangelands? wildfire risk zoning using GIS and AHP techniques. *Casp. J. Environ. Sci.* **2012**, *10*, 43–52.

47. Rasooli, S.B.; Bonyad, A.E.; Pir Bavaghar, M. Forest fire vulnerability map using remote sensing data, GIS and AHP analysis (Case study: Zarivar Lake surrounding area). *Casp. J. Environ. Sci.* **2018**, *16*, 369–377.
48. Zarekar, A.; Zamani, B.K.; Ghorbani, S.; Moalla, M.A.; Jafari, H. Mapping spatial distribution of forest fire using MCDM and GIS (case study: Three forest zones in Guilan Province). *Iran. J. For. Poplar Res.* **2013**, *21*, 218–230.
49. Bui, D.T.; Bui, Q.-T.; Nguyen, Q.-P.; Pradhan, B.; Nampak, H.; Trinh, P.T. A hybrid artificial intelligence approach using GIS-based neural-fuzzy inference system and particle swarm optimization for forest fire susceptibility modeling at a tropical area. *Agric. For. Meteorol.* **2017**, *233*, 32–44.
50. Gheshlaghi, H.A. Using GIS to develop a model for forest fire risk mapping. *J. Indian Soc. Remote Sens.* **2019**, *47*, 1173–1185. [CrossRef]
51. Martínez, J.; Vega-Garcia, C.; Chuvieco, E. Human-caused wildfire risk rating for prevention planning in Spain. *J. Environ. Manag.* **2009**, *90*, 1241–1252. [CrossRef]
52. Jurdao, S.; Chuvieco, E.; Arevalillo, J.M. Modelling fire ignition probability from satellite estimates of live fuel moisture content. *Fire Ecol.* **2012**, *8*, 77–97. [CrossRef]
53. Mohammadi, F.; Bavaghar, M.P.; Shabanian, N. Forest Fire Risk Zone Modeling Using Logistic Regression and GIS: An Iranian Case Study. *Small-Scale For.* **2014**, *13*, 117–125. [CrossRef]
54. Tien Bui, D.; Le, K.-T.T.; Nguyen, V.C.; Le, H.D.; Revhaug, I. Tropical forest fire susceptibility mapping at the Cat Ba National Park Area, Hai Phong City, Vietnam, using GIS-based kernel logistic regression. *Remote Sens.* **2016**, *8*, 347. [CrossRef]
55. Vasilakos, C.; Kalabokidis, K.; Hatzopoulos, J.; Matsinos, I. Identifying wildland fire ignition factors through sensitivity analysis of a neural network. *Nat. Hazards* **2009**, *50*, 125–143. [CrossRef]
56. Pierce, A.D.; Farris, C.A.; Taylor, A.H. Use of random forests for modeling and mapping forest canopy fuels for fire behavior analysis in Lassen Volcanic National Park, California, USA. *For. Ecol. Manag.* **2012**, *279*, 77–89. [CrossRef]
57. Mirdeilami, T.; Shataee, S.H.; Kavoosi, M.R. Forest fire risk zone mapping in the Golestan national park using regression logistic method. *J. Wood For. Sci. Technol.* **2015**, *22*, 1–16.
58. Srivastava, P.K.; Petropoulos, G.P.; Gupta, M.; Singh, S.K.; Islam, T.; Loka, D. Deriving forest fire probability maps from the fusion of visible/infrared satellite data and geospatial data mining. *Model. Earth Syst. Environ.* **2019**, *5*, 627–643. [CrossRef]
59. Salar, S.G. *Geomorphic Analysis for Water Harvesting Using GIS Technique in Selected Basins/Garmiyan Iraqi Kurdistan Region*; University of Sulaimani: Sulaymaniyah, Iraq, 2013.
60. Salar, S.G.; Othman, A.A.; Hasan, S.E. Identification of suitable sites for groundwater recharge in Awaspi watershed using GIS and remote sensing techniques. *Environ. Earth Sci.* **2018**, *77*, 701. [CrossRef]
61. Kummerow, C.; Barnes, W.; Kozu, T.; Shiue, J.; Simpson, J. The Tropical Rainfall Measuring Mission (TRMM) sensor package. *J. Atmos. Ocean. Technol.* **1998**, *15*, 809–817. [CrossRef]
62. NCEP Climate Forecast System Reanalysis (CFSR) Global Weather Data. Available online: https://swat.tamu.edu/data/cfsr (accessed on 13 August 2021).
63. Rouse, J.W.; Haas, R.H.; Schelle, J.A.; Deering, D.W.; NASA/GSFC. *Monitoring the Vernal Advancement or Retrogradation of Natural Vegetation*; NASA: Greenbelt, MD, USA, 1974.
64. Moore, I.D.; Grayson, R.B.; Ladson, A.R. Digital terrain modelling: A review of hydrological, geomorphological, and biological applications. *Hydrol. Process.* **1991**, *5*, 3–30. [CrossRef]
65. Weiss, A. Topographic position and landforms analysis, Poster presentation. In Proceedings of the ESRI user conference, San Diego, CA, USA, 9–13 July 2001; pp. 9–13.
66. Zeng, T.; Hudson, J.; Kay, S.; Laginestra, E.; Authority, S.O.P. A fuzzy GIS approach to fire risk assessment: A case study of Sydney Olympic Park, Australia. In Proceedings of the Spatial Sciences Conferences, Sydney, Australia, January 2003; Volume 18.
67. Sayad, Y.O.; Mousannif, H.; Al Moatassime, H. Predictive modeling of wildfires: A new dataset and machine learning approach. *Fire Saf. J.* **2019**, *104*, 130–146. [CrossRef]
68. Koutsias, N.; Xanthopoulos, G.; Founda, D.; Xystrakis, F.; Nioti, F.; Pleniou, M.; Mallinis, G.; Arianoutsou, M. On the relationships between forest fires and weather conditions in Greece from long-term national observations (1894–2010). *Int. J. Wildl. Fire* **2012**, *22*, 493–507. [CrossRef]
69. Faramarzi, H.; Hosseini, S.M.; Gholamalifard, M. Fire hazard zoning in national golestan park using logistic regression and GIS. *J. Geogr. Environ. Hazards* **2014**, *3*, 73–90.
70. Sakr, G.E.; Elhajj, I.H.; Mitri, G. Efficient forest fire occurrence prediction for developing countries using two weather parameters. *Eng. Appl. Artif. Intell.* **2011**, *24*, 888–894. [CrossRef]
71. Rajabi, M.; Alesheikh, A.; Chehreghan, A.; Gazmeh, H. An innovative method for forest fire risk zoning map using fuzzy inference system and GIS. *Int. J. Sci. Technol. Res.* **2013**, *2*, 57–64.
72. Saklani, P. *Forest Fire Risk Zonation: A Case Study Pauri Garhwal*; ITC: Uttrakhand, India, 2008.
73. Behzadi, H.; Mohtashamnia, S.; Gharedaghi, H. Rangelands and forests fire risk zoning using GIS and AHP model (case study: Bamu National Park, Fars province). *Iran. J. Range Desert Res.* **2019**, *25*, fa817–fa827.
74. Jenness, J.S. The Effects of Fire on Mexican Spotted Owls in Arizona and New Mexico. 2000. Available online: http://www.jennessent.com/Literature/Thesis/literature_review.htm#Forest%20Service%20Management%20Plans (accessed on 3 February 2022).

75. Othman, A.A.; Al-Maamar, A.F.; Al-Manmi, D.A.M.; Veraldo, L.; Hasan, S.E.; Obaid, A.K.; Al-Quraishi, A.M.F. GIS-based modeling for selection of dam sites in the Kurdistan Region, Iraq. *ISPRS Int. J. Geo-Inf.* **2020**, *9*, 244. [CrossRef]
76. Othman, A.A.; Obaid, A.K.; Amin Al-Manmi, D.A.M.; Al-Maamar, A.F.; Hasan, S.E.; Liesenberg, V.; Shihab, A.T.; Al-Saady, Y.I. New insight on soil loss estimation in the northwestern region of the Zagros fold and Thrust Belt. *ISPRS Int. J. Geo-Inf.* **2021**, *10*, 59. [CrossRef]
77. Saha, S.; Moorthi, S.; Pan, H.-L.; Wu, X.; Wang, J.; Nadiga, S.; Tripp, P.; Kistler, R.; Woollen, J.; Behringer, D. The NCEP climate forecast system reanalysis. *Bull. Am. Meteorol. Soc.* **2010**, *91*, 1015–1058. [CrossRef]
78. Sissakian, V.K.; Fouad, S.F.A. *The Geology of Sulaimaniya Quadrangle Sheet No. NI-38-3, Scale 1:250,000*; GEOSURV: Baghdad, Iraq, 2008.
79. Al-Rubaiay, A.T.; Al-Dulaimi, T.Y. *Series of Land Use Land Cover Maps of Iraq Scale 1:250,000, Sulaimaniya Quadrangle Sheet NI–38–3 (LULCM 10)*; GEOSURV: Baghdad, Iraq, 2012.
80. Heydari, M.; Poorbabaei, H.; Esmaaelzade, O. Indicator plant species in monitoring forest soil conditions using logistic regression model in Zagros Oak (Quercus brantii var. persica) forest ecosystems, Ilam city. *J. Plant Res.* **2015**, *27*, 811–828.
81. Eastman, J.R. *IDRISI Taiga Guide to GIS and Image Processing*; Clark Labs Clark University: Worcester, MA, USA, 2009.
82. Pontius, R.G., Jr.; Schneider, L.C. Land-cover change model validation by an ROC method for the Ipswich watershed, Massachusetts, USA. *Agric. Ecosyst. Environ.* **2001**, *85*, 239–248. [CrossRef]
83. Othman, A.A.; Gloaguen, R.; Andreani, L.; Rahnama, M. Improving landslide susceptibility mapping using morphometric features in the Mawat area, Kurdistan Region, NE Iraq: Comparison of different statistical models. *Geomorphology* **2018**, *319*, 147–160. [CrossRef]
84. Youssef, A.M.; Pourghasemi, H.R.; Pourtaghi, Z.S.; Al-Katheeri, M.M. Landslide susceptibility mapping using random forest, boosted regression tree, classification and regression tree, and general linear models and comparison of their performance at Wadi Tayyah Basin, Asir Region, Saudi Arabia. *Landslides* **2016**, *13*, 839–856. [CrossRef]
85. Jaafari, A.; Najafi, A.; Rezaeian, J.; Sattarian, A.; Ghajar, I. Planning road networks in landslide-prone areas: A case study from the northern forests of Iran. *Land Use Policy* **2015**, *47*, 198–208. [CrossRef]
86. Shrestha, R.; Di, L.; Yu, E.G.; Kang, L.; SHAO, Y.; BAI, Y. Regression model to estimate flood impact on corn yield using MODIS NDVI and USDA cropland data layer. *J. Integr. Agric.* **2017**, *16*, 398–407. [CrossRef]
87. Loveridge, M.; Rahman, A. Effects of Probability-Distributed Losses on Flood Estimates Using Event-Based Rainfall-Runoff Models. *Water* **2021**, *13*, 2049. [CrossRef]
88. Bergmeir, C.; Benítez, J.M. On the use of cross-validation for time series predictor evaluation. *Inf. Sci.* **2012**, *191*, 192–213. [CrossRef]
89. Bennett, M.; Fitzgerald, S.A.; Parker, B.; Main, M.L.; Perleberg, A.; Schnepf, C.; Mahoney, R.L. *Reducing Fire Risk on Your Forest Property*; Oregon State University: Corvallis, OR, USA, 2010.
90. Lecina-Diaz, J.; Alvarez, A.; Retana, J. Extreme fire severity patterns in topographic, convective and wind-driven historical wildfires of Mediterranean pine forests. *PLoS ONE* **2014**, *9*, e85127. [CrossRef]
91. Oliveira, S.; Pereira, J.M.C.; San-Miguel-Ayanz, J.; Lourenço, L. Exploring the spatial patterns of fire density in Southern Europe using Geographically Weighted Regression. *Appl. Geogr.* **2014**, *51*, 143–157. [CrossRef]
92. Adab, H.; Kanniah, K.D.; Solaimani, K. Modelling static fire hazard in a semi-arid region using frequency analysis. *Int. J. Wildl. Fire* **2015**, *24*, 763–777. [CrossRef]
93. Li, R.; Wang, N. Landslide susceptibility mapping for the Muchuan county (China): A comparison between bivariate statistical models (woe, ebf, and ioe) and their ensembles with logistic regression. *Symmetry* **2019**, *11*, 762. [CrossRef]
94. Gholami, P.; Ghorbani, J.; Abbasi, H. Effect of fire vegetation on some properties of soil in rangelands of Bamo national park in Shiraz. *Nat. Ecosyst. Iran* **2014**, *5*, 41–50.
95. Rafiee, F.; Jankju, M.; Ejtehadi, H. Investigation on tolerant, adapted and sensitive plant traits to chronological wildfires in a semiarid rangeland. *Iran. J. Range Desert Res.* **2015**, *22*, Pe73–Pe84.
96. Oliveira, C.; Ferreira, R.; da Silva, J.; Lima, R.; Silva, E.; Silva, A.; Lucena, J.; dos Santos, N.; Lopes, I.; Pessoa, M.; et al. Modeling and Spatialization of Biomass and Carbon Stock Using LiDAR Metrics in Tropical Dry Forest, Brazil. *Forests* **2021**, *12*, 473. [CrossRef]
97. Fernández-Guisuraga, J.M.; Calvo, L.; Fernandes, P.M.; Suárez-Seoane, S. Short-Term Recovery of the Aboveground Carbon Stock in Iberian Shrublands at the Extremes of an Environmental Gradient and as a Function of Burn Severity. *Forests* **2022**, *13*, 145. [CrossRef]
98. Zhang, F.; Zhou, G. Estimation of vegetation water content using hyperspectral vegetation indices: A comparison of crop water indicators in response to water stress treatments for summer maize. *BMC Ecol.* **2019**, *19*, 18. [CrossRef]
99. González-Olabarria, J.-R.; Rodriguez, F.; Fernández-Landa, A.; Mola-Yudego, B. Mapping fire risk in the Model Forest of Urbión (Spain) based on airborne LiDAR measurements. *For. Ecol. Manag.* **2012**, *282*, 149–156. [CrossRef]
100. Reddy, C.S.; Bird, N.G.; Sreelakshmi, S.; Manikandan, T.M.; Asra, M.; Krishna, P.H.; Jha, C.S.; Rao, P.V.N.; Diwakar, P.G. Identification and characterization of spatio-temporal hotspots of forest fires in South Asia. *Environ. Monit. Assess.* **2019**, *191*, 791. [CrossRef]

101. Avitabile, S.C.; Callister, K.E.; Kelly, L.T.; Haslem, A.; Fraser, L.; Nimmo, D.G.; Watson, S.J.; Kenny, S.A.; Taylor, R.S.; Spence-Bailey, L.M.; et al. Systematic fire mapping is critical for fire ecology, planning and management: A case study in the semi-arid Murray Mallee, south-eastern Australia. *Landsc. Urban Plan.* **2013**, *117*, 81–91. [CrossRef]
102. Bernier, P.Y.; Gauthier, S.; Jean, P.-O.; Manka, F.; Boulanger, Y.; Beaudoin, A.; Guindon, L. Mapping Local Effects of Forest Properties on Fire Risk across Canada. *Forests* **2016**, *7*, 157. [CrossRef]
103. Carvalheiro, L.C.; Bernardo, S.O.; Orgaz, M.D.M.; Yamazaki, Y. Forest Fires Mapping and Monitoring of current and past forest fire activity from Meteosat Second Generation Data. *Environ. Model. Softw.* **2010**, *25*, 1909–1914. [CrossRef]
104. Chen, D.; Pereira, J.M.C.; Masiero, A.; Pirotti, F. Mapping fire regimes in China using MODIS active fire and burned area data. *Appl. Geogr.* **2017**, *85*, 14–26. [CrossRef]
105. Dlamini, W.M. Application of Bayesian networks for fire risk mapping using GIS and remote sensing data. *GeoJournal* **2011**, *76*, 283–296. [CrossRef]
106. Duarte, L.; Teododo, A.C. An easy, accurate and efficient procedure to create forest fire risk maps using the SEXTANTE plugin Modeler. *J. For. Res.* **2016**, *27*, 1361–1372. [CrossRef]
107. Hudak, A.T.; Bright, B.C.; Pokswinski, S.M.; Loudermilk, E.L.; O'Brien, J.J.; Hornsby, B.S.; Klauberg, C.; Silva, C.A. Mappingforest structure and composition from low-density LiDAR for informed forest, fuel, and fire management at Eglin Air Force Base, Florida, USA. *Can. J. Remote Sens.* **2016**, *42*, 411–427. [CrossRef]
108. Kumar, S.; Das Bairagi, G.; Kumar, A. Identifying triggers for forest fire and assessing fire susceptibility of forests in Indian western Himalaya using geospatial techniques. *Nat. Hazards* **2015**, *78*, 203–217. [CrossRef]
109. Lampin-Maillet, C.; Jappiot, M.; Long, M.; Bouillon, C.; Morge, D.; Ferrier, J.-P. Mapping wildland-urban interfaces at large scales integrating housing density and vegetation aggregation for fire prevention in the South of France. *J. Environ. Manag.* **2010**, *91*, 732–741. [CrossRef] [PubMed]
110. Merino-de-Miguel, S.; Huesca, M.; González-Alonso, F. Modis reflectance and active fire data for burn mapping and assessment at regional level. *Ecol. Modell.* **2010**, *221*, 67–74. [CrossRef]
111. Mitri, G.H.; Gitas, I.Z. Mapping post-fire forest regeneration and vegetation recovery using a combination of very high spatial resolution and hyperspectral satellite imagery. *Int. J. Appl. Earth Obs. Geoinf.* **2013**, *20*, 60–66. [CrossRef]
112. Molina, J.R.; González-Cabán, A.; y Silva, F.R. Wildfires impact on the economic susceptibility of recreation activities: Application in a Mediterranean protected area. *J. Environ. Manag.* **2019**, *245*, 454–463. [CrossRef]
113. Ruiz, J.A.M.; Riaño, D.; Arbelo, M.; French, N.H.F.; Ustin, S.L.; Whiting, M.L. Burned area mapping time series in Canada (1984–1999) from NOAA-AVHRR LTDR: A comparison with other remote sensing products and fire perimeters. *Remote Sens. Environ.* **2012**, *117*, 407–414. [CrossRef]
114. Morton, D.C.; DeFries, R.S.; Nagol, J.; Souza, C.M., Jr.; Kasischke, E.S.; Hurtt, G.C.; Dubayah, R. Mapping canopy damage from understory fires in Amazon forests using annual time series of Landsat and MODIS data. *Remote Sens. Environ.* **2011**, *115*, 1706–1720. [CrossRef]
115. Naderpour, M.; Rizeei, H.M.; Khakzad, N.; Pradhan, B. Forest fire induced Natech risk assessment: A survey of geospatial technologies. *Reliab. Eng. Syst. Saf.* **2019**, *191*, 106558. [CrossRef]
116. Nandy, S.; Singh, C.; Das, K.K.; Kingma, N.C.; Kushwaha, S.P.S. Environmental vulnerability assessment of eco-development zone of Great himalayan National Park, himachal Pradesh, India. *Ecol. Indic.* **2015**, *57*, 182–195. [CrossRef]
117. Potapov, P.; Turubanova, S.; Hansen, M.C. Regional-scale boreal forest cover and change mapping using Landsat data composites for European Russia. *Remote Sens. Environ.* **2011**, *115*, 548–561. [CrossRef]
118. Sahana, M.; Ganaie, T.A. GIS-based landscape vulnerability assessment to forest fire susceptibility of Rudraprayag district, Uttarakhand, India. *Environ. Earth Sci.* **2017**, *76*, 676. [CrossRef]
119. Saranya, K.R.L.; Reddy, C.S.; Rao, P.V.V.P.; Jha, C.S. Decadal time-scale monitoring of forest fires in Similipal Biosphere Reserve, India using remote sensing and GIS. *Environ. Monit. Assess* **2014**, *186*, 3283–3296. [CrossRef]
120. Weisberg, P.J.; Ko, D.; Py, C.; Bauer, J.M. Modeling fire and landform influences on the distribution of old-growth pinyon-juniper woodland. *Landsc. Ecol.* **2008**, *23*, 931–943. [CrossRef]
121. Whitman, E.; Rapaport, E.; Sherren, K. Modeling fire susceptibility to delineate wildland–urban interface for municipal-scale fire risk management. *Environ. Manag.* **2013**, *52*, 1427–1439. [CrossRef]
122. Yang, W.; Zhang, S.; Tang, J.; Bu, K.; Yang, J.; Chang, L. A MODIS time series data based algorithm for mapping forest fire burned area. *Chin. Geogr. Sci.* **2013**, *23*, 344–352. [CrossRef]
123. You, W.; Lin, L.; Wu, L.; Ji, Z.; Zhu, J.; Fan, Y.; He, D. Geographical information system-based forest fire risk assessment integrating national forest inventory data and analysis of its spatiotemporal variability. *Ecol. Indic.* **2017**, *77*, 176–184. [CrossRef]
124. Ziccardi, L.G.; Thiersch, C.R.; Yanai, A.M.; Fearnside, P.M.; Ferreira-Filho, P.J. Forest fire risk indices and zoning of hazardous areas in Sorocaba, São Paulo state, Brazil. *J. For. Res.* **2020**, *31*, 581–590. [CrossRef]
125. Cao, Y.; Wang, M.; Liu, K. Wildfire susceptibility assessment in Southern China: A comparison of multiple methods. *Int. J. Disaster Risk Sci.* **2017**, *8*, 164–181. [CrossRef]
126. Pourghasemi, H.R.; Beheshtirad, M.; Pradhan, B. A comparative assessment of prediction capabilities of modified analytical hierarchy process (M-AHP) and Mamdani fuzzy logic models using Netcad-GIS for forest fire susceptibility mapping. *Geomat. Nat. Hazards Risk* **2016**, *7*, 861–885. [CrossRef]

127. Eskandari, S. A new approach for forest fire risk modeling using fuzzy AHP and GIS in Hyrcanian forests of Iran. *Arab. J. Geosci.* **2017**, *10*, 190. [CrossRef]
128. Li, X.; Lanorte, A.; Telesca, L.; Song, W.; Lasaponara, R. Assessment of MODIS-Based NDVI-Derived Index for Fire Susceptibility Estimation in Northern China. In Proceedings of the International Conference on Computational Science and Its Applications, Banff, AB, Canada, 22–25 June 2015; pp. 193–203.
129. Liu, W.; Wang, S.; Zhou, Y.; Wang, L.; Zhu, J.; Wang, F. Lightning-caused forest fire risk rating assessment based on case-based reasoning: A case study in DaXingAn Mountains of China. *Nat. Hazards* **2016**, *81*, 347–363. [CrossRef]
130. Liu, Q.; Shan, Y.; Shu, L.; Sun, P.; Du, S. Spatial and temporal distribution of forest fire frequency and forest area burnt in Jilin Province, Northeast China. *J. For. Res.* **2018**, *29*, 1233–1239. [CrossRef]
131. Tehrany, M.S.; Jones, S.; Shabani, F.; Martínez-Álvarez, F.; Bui, D.T. A novel ensemble modeling approach for the spatial prediction of tropical forest fire susceptibility using LogitBoost machine learning classifier and multi-source geospatial data. *Arch. Meteorol. Geophys. Bioclimatol. Ser. B* **2018**, *137*, 637–653. [CrossRef]